

# Evolution of the central Garlock fault zone, California: A major sinistral fault embedded in a dextral plate margin

Joseph E. Andrew<sup>1,†</sup>, J. Douglas Walker<sup>1</sup>, and Francis C. Monastero<sup>2</sup>

<sup>1</sup>Department of Geology, University of Kansas, Lawrence, Kansas 66045, USA

<sup>2</sup>8597 Timaru Trail, Reno, Nevada 89523, USA

## ABSTRACT

The Garlock fault is an integral part of the plate-boundary deformation system inboard of the San Andreas fault (California, USA); however, the Garlock is transversely oriented and has the opposite sense of shear. The slip history of the Garlock is critical for interpreting the deformation of the through-going dextral shear of the Walker Lane belt–Eastern California shear zone. The Lava Mountains–Summit Range (LMSR), located along the central Garlock fault, is a Miocene volcanic center that holds the key to unraveling the fault slip and development of the Garlock. The LMSR is also located at the intersection of the NNW-striking dextral Blackwater fault and contains several sinistral WSW-striking structures that provide a framework for establishing the relationship between the sinistral Garlock fault system and the dextral Eastern California shear zone. New field mapping and geochronology data (<sup>40</sup>Ar/<sup>39</sup>Ar and U-Pb) show five distinct suites of volcanic-sedimentary rock units in the LMSR overlain by Pliocene exotic-clast conglomerates. This stratigraphy coupled with fifteen fault slip markers define a three-stage history for the central Garlock fault system of 11–7 Ma, 7–3.8 Ma, and 3.8–0 Ma. Pliocene to recent slip occurs in a ~12-km-wide zone and accounts for ~33 km or 51% of the total 64 km of left-lateral offset on the Garlock fault in the vicinity of the LMSR since 3.8 Ma. This history yields slip rates of 6–9 mm/yr for the younger stage and slower rates for older stages. The LMSR internally accommodates northwest-directed dextral slip associated with the Eastern California shear zone–Walker Lane belt via multiple processes of lateral tectonic escape, folding, normal faulting,

and the creation of new faults. The geologic slip rates for the Garlock fault in the LMSR match with and explain along-strike variations in neotectonic rates.

## INTRODUCTION

A quarter of the North American to Pacific plate displacement is actively accommodated by dextral shear in eastern California (Miller et al., 2001). The Garlock fault (Fig. 1 inset map) is an active large-magnitude sinistral-slip fault (Hess, 1910; Hulin, 1925; Dibblee, 1952; Smith, 1962) embedded in and perpendicular to this zone of dextral shear. The Garlock is a fundamental structure in this deformation zone, as it separates the dextral transpressive Eastern California shear zone to its south (Dokka and Travis, 1990) from the dextral transtensional Walker Lane belt to its north (Stewart, 1988). Active NNW-striking dextral fault systems both north and south of the Garlock fault have abundant seismicity (Unruh and Hauksson, 2009) and offsets of 2–12 km (Monastero et al., 2002; Glazner et al., 2000; Oskin and Iriondo, 2004; Casey et al., 2008; Frankel et al., 2008; Andrew and Walker, 2009). Geodetic data show that dextral shear crosses the Garlock fault unimpeded (Peltzer et al., 2001; Gan et al., 2003) with an additional component of northwest-directed extension north of the Garlock fault (Savage et al., 2001). Despite the activity and significant offsets on the NNW-striking faults, these faults nowhere cut the Garlock fault (Noble, 1926). The Garlock fault has a curved trace, with its central and eastern segments rotated clockwise relative to its straight western segment (Fig. 1). This change in strike has been interpreted as oroclinal bending that accommodates dextral shear in the Mojave Desert (Garfunkel, 1974; Schermer et al., 1996; Guest et al., 2003; Gan et al., 2003). Most models of this oroclinal bending are based on dextral shear and counterclockwise rotation of crustal blocks, but the corners of these blocks with the Garlock fault have not been studied.

A major hurdle to understanding the tectonics of the Garlock fault has been establishing a detailed slip history, because the age of all of the known slip markers predate the initiation of slip. The total slip on the Garlock fault is ~64 km using offset pre-Cenozoic features (see Fig. 1 and Table 1 for descriptions and references); however, slip initiated after 17 Ma (Monastero et al., 1997) and possibly at 11 Ma (Burbank and Whistler, 1987; Blythe and Longinotti, 2013). The Garlock has neotectonic slip rates of 4.5–14 mm/yr (Clark and Lajoie, 1974; McGill and Sieh, 1993; McGill et al., 2009; Rittase et al., 2014), but most of these rates are too rapid if they are applied to the 11 m.y. history of the Garlock fault (64 km over 11 m.y. = 5.8 mm/yr).

This paper presents new stratigraphic, structural, and geochronologic data to define a detailed history for the Garlock fault. This study focuses on the central segment of fault in the Lava Mountains–Summit Range (LMSR) area, a Miocene volcanic center located immediately adjacent to the Garlock fault (Smith, 1964; Dibblee, 1967; Smith et al., 2002). Previous workers suggested that Miocene and younger strata in the LMSR can be correlated across the fault (Carter, 1994; Smith et al., 2002; Frankel et al., 2008), thus offering the potential to understand the slip history in detail. It is also an important study site because it contains the northern terminus of the dextral Blackwater fault, a major fault of the Eastern California shear zone. This paper describes the stratigraphy of the LMSR and the geometry and kinematics of the structures, to identify numerous offset markers to restore fault movements. The goal of this paper is to use these data and interpretations to construct the slip history of the Garlock and associated faults. This history is needed to resolve the initiation of slip on the Garlock fault system and the current structural configuration, and to evaluate major changes in slip magnitude, fault geometry, and deformation style. We consider the implications of the current structural configuration to create a model

<sup>†</sup>E-mail: jeandrew@ku.edu

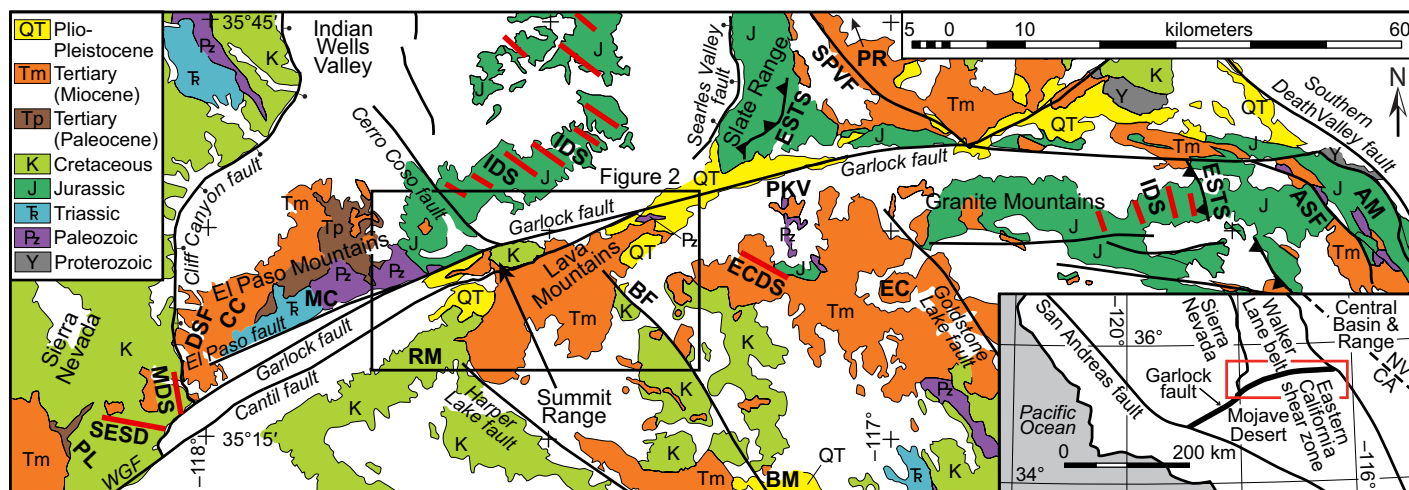


**Figure 1.** Simplified geologic map of the central and eastern Garlock fault (California, USA). Inset map shows the Garlock fault (thickest line), Figure 1 area (red line), geologic provinces, other features, and the border between California (CA) and Nevada (NV). Previously published total offset constraints for the Garlock fault are shown in bold text (see Table 1 for abbreviations and descriptions). Fault abbreviations: BF—Blackwater fault; WGF—western Garlock fault; BM—Black Mountain; DSF—Dove Spring Formation; ECDS—Eagle Crag dike swarm; MDS—megacrystic dike swarm; and SESD—Southeast Sierra dikes. Geology modified from Walker et al. (2002). Holocene and upper Pleistocene units are shown as white.

**TABLE 1.** PUBLISHED CONSTRAINTS OF LEFT-LATERAL OFFSET ON THE GARLOCK FAULT

Feature	Authors	Amount (km)*	Details	Labels†	
				North	South
Independence dike swarm	Smith (1962)	64	Late Jurassic Independence dike swarm (IDS) in the Spangler Hills with dikes in the Granite Mountains	IDS	IDS
Fault domain boundary	Michael (1966)	74	Eastern boundary of domain of northwest-striking faults; Piute Line (PL) in the southeastern Sierra Nevada and Blackwater fault (BF) in the northern Mojave Desert	PL	BF
Rand Schist	Dibblee (1967)	72	Late Cretaceous Rand Schist in the Rand Mountains (RM) and in the southern Sierra Nevada	#	RM
East Sierran thrust system	Smith et al. (1968); Davis and Burchfiel (1973)	52–64	Jurassic East Sierran thrust system (ESTS) in the southern Slate Range and in the Granite Mountains	ESTS	ESTS
Eugeoclinal Paleozoic rocks	Smith and Ketner (1970); Carr et al. (1997)	48–64	Paleozoic eugeoclinal metasedimentary and metavolcanic rocks with thrust faults in Mesquite Canyon (MC) of the El Paso Mountains and south of Pilot Knob Valley (PKV)	MC	PKV
Basal passive margin sequence	Jahns et al. (1971)	48–64	Neoproterozoic to early Paleozoic miogeoclinal sequences in the Panamint Range (PR) and Avawatz Mountains (AM)	PR	AM
Fault that juxtaposes Mesozoic and Proterozoic rocks	Davis and Burchfiel (1973)	64	NNW-striking faults that juxtapose Mesozoic rocks with Proterozoic rocks; Southern Panamint Valley fault (SPVF) with the Arrastre Spring fault (ASF) in the Avawatz Mountains	SPVF	ASF
Early Miocene volcanic fields	Monastero et al. (1997)	64	Early Miocene Cudahy Camp Formation (CC) of Loomis and Burbank (1988) with the Eagle Crag Volcanics (EC) of Sabin (1994)	CC	EC

\*Amount—Left-lateral offset along the Garlock fault determined for each feature, either as best estimated or as minimum and maximum amounts.

†Labels—Labels for these features on Figure 1. North and south refer to the offset features on the north and south sides of the Garlock fault.

\*This location is west of the area of Figure 1.

of dextral shear accommodation without dextral faults cutting the Garlock fault. Lastly, we compare our interpreted long-term slip rates to published neotectonic rates along the Garlock.

**STRATIGRAPHY**

Despite the volume of previous work, there were still many undated rock units and uncertainties regarding the order and stratigraphic relationships of the Miocene units and structures in the LMSR. New detailed geologic mapping of this area (Andrew et al., 2014; summarized

and simplified on Fig. 2) and geochronologic analysis (locations on Fig. 2) of key rock units were used to better define and delineate the stratigraphy of the area (Fig. 3) as well as reveal the details of faulting.

**Geochronology**

We establish age constraints in the LMSR by dating samples using the <sup>40</sup>Ar/<sup>39</sup>Ar and U-Pb zircon geochronology methods and by reinterpreting previously published <sup>40</sup>Ar/<sup>39</sup>Ar ages of Smith et al. (2002). An additional sample

was collected in the Sierra Nevada (MDS on Fig. 1). New volcanic rock samples from the LMSR (Table DR1 in the GSA Data Repository<sup>1</sup>) were analyzed by the <sup>40</sup>Ar/<sup>39</sup>Ar geochronology step-heating method, mostly at the New Mexico Geochronology Research Laboratory (analytical methods in Heizler et al. [1999] and Brueseke et al. [2007]) and one

<sup>1</sup>GSA Data Repository item 2014297, additional geochronologic data, is available at <http://www.geosociety.org/pubs/ft2014.htm> or by request to [editing@geosociety.org](mailto:editing@geosociety.org).

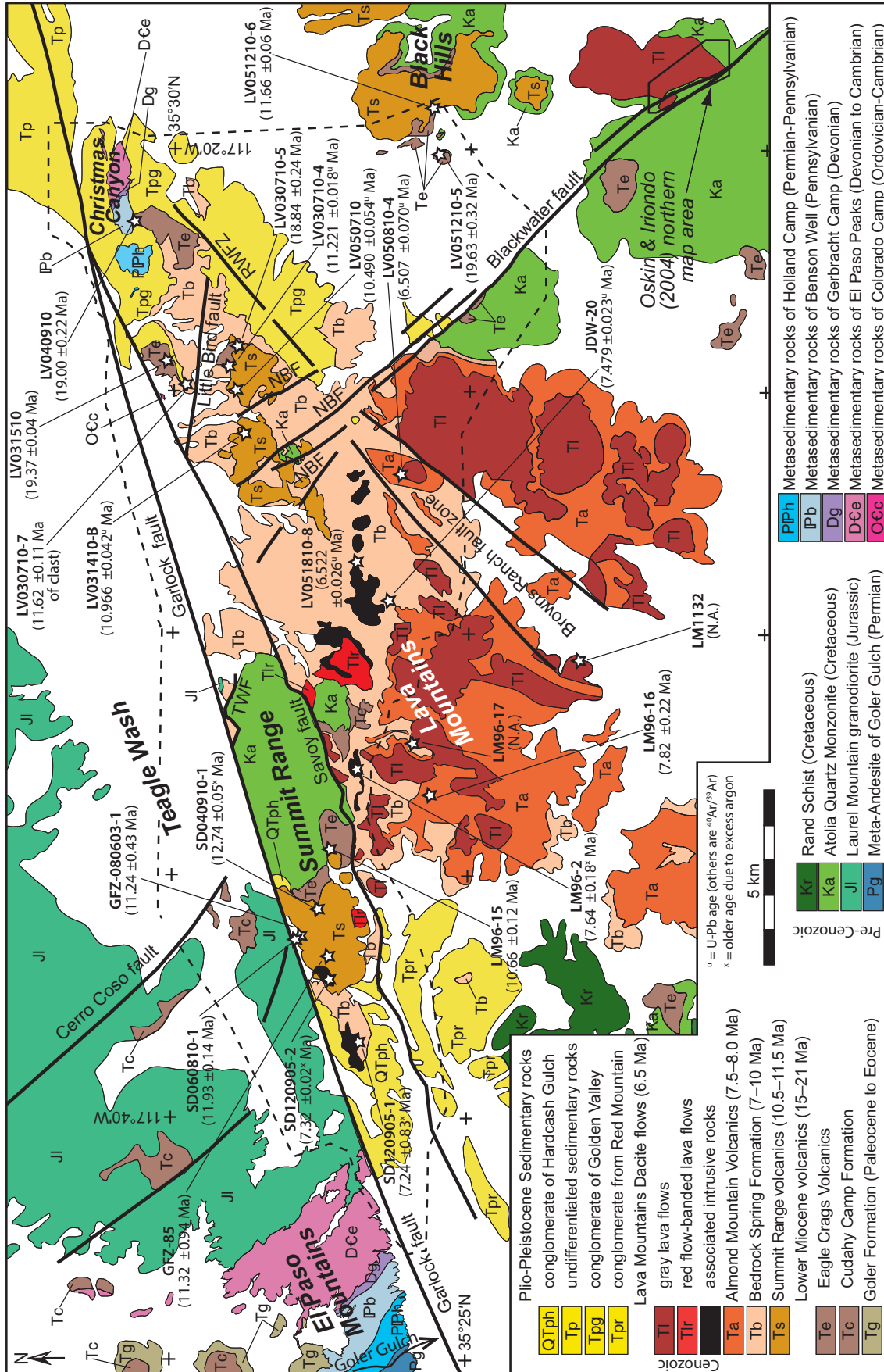
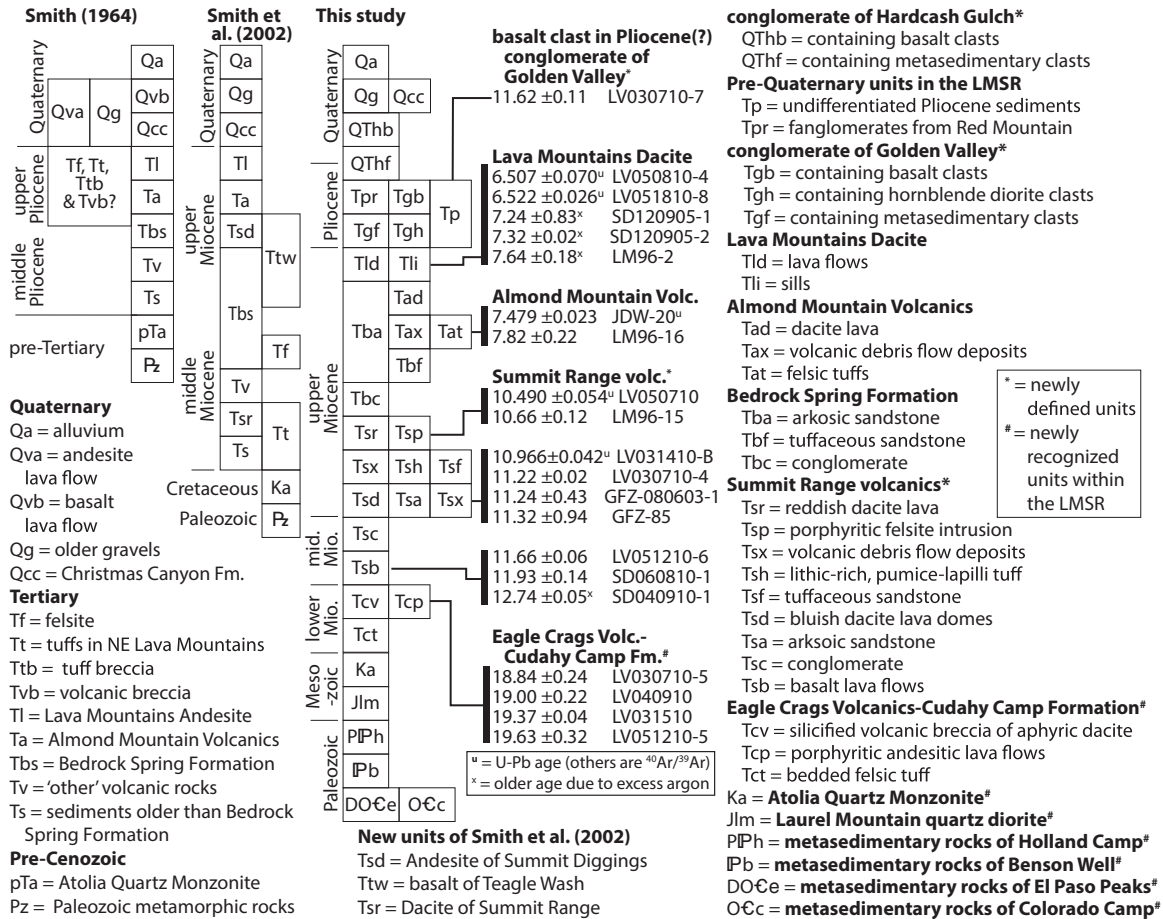


Figure 2. Simplified geologic map of the Lava Mountains-Summit Range. Data from inside the dashed line are from Andrew et al. (2014); additional data are from Dibblee (1967), Carr et al. (1997), and Walker et al. (2002). Geochronologic sample locations are denoted by stars with sample name and interpreted age in parentheses. Faults are thick lines. Fault abbreviations: NBF—northern Blackwater fault; RWFZ—Randsburg Wash fault zone; TWF—Teagle Wash fault. Younger Pleistocene and Holocene units are shown as white.





**Figure 3. Stratigraphic interpretations for correlation of units for the Lava Mountains–Summit Range (LMSR). New and newly interpreted geochronologic constraints are listed to the right with the age (in Ma) and sample name (for age interpretations, see Tables 2 and 3 and Figs. 4, 5, and 6).**

other at the Massachusetts Institute of Technology (MIT; analytical methods in Hodges et al. [1994] and Snyder and Hodges [2000]). A sample containing sanidine was analyzed by single crystal fusion. Step-heating results were interpreted using plateau and inverse isochron methods (Fig. 4; see Table 2 for interpretation of <sup>40</sup>Ar/<sup>39</sup>Ar age data) using the software Isoplot (Ludwig, 2012). Six samples of zircon from felsic rocks were analyzed by chemical abrasion thermal ionization mass spectrometry (CA-TIMS) at the Isotope Geology Laboratory at the University of Kansas (Table DR2). Samples were annealed and leached following the protocols of Mattinson (2005), then spiked with EarthTime ET535 tracer and dissolved using standard U-Pb double pressure-vessel digestion procedures. Column-purified U and Pb were run together on a VG Sector TIMS run in single-collector ion-counting mode for Pb and multicollector static mode for U. Data were reduced and interpreted using Tripoli and U-Pb\_Redux software (Bowring et al.,

2011). Compiled single zircon crystal fractions give crystallization ages of these rocks (Table 3; Fig. 5).

We reinterpret the step-heating <sup>40</sup>Ar/<sup>39</sup>Ar analyses of Smith et al. (2002); neither the data nor interpretive plots were published, but the data were available from author Monastero (Table DR3), who was a collaborator on the Smith et al. (2002) work. These samples were analyzed at the MIT lab. Our rationale for reinterpreting these ages is that hornblende and biotite from the same samples yielded very different ages (e.g., Fig. 6E), but Smith et al. (2002) interpreted the ages based on the hornblende ages alone. The <sup>40</sup>Ar/<sup>39</sup>Ar hornblende spectra show evidence of excess argon (i.e., saddle-shaped plateau and non-atmospheric <sup>40</sup>Ar/<sup>36</sup>Ar intercept values on Fig. 6D) (e.g., Lanphere and Dalrymple, 1976; Harrison and McDougall, 1981), so we reinterpret the ages of these rocks (Table 2B) by examining plots of age spectra and inverse isochrons using the biotite analyses (Fig. 6).

### Stratigraphic Units

#### Paleozoic Metasedimentary Rocks

Coherent basement of metasedimentary rocks occurs in the Christmas Canyon area (Figs. 2 and 7). These rocks have relatively low metamorphic grades and consist mostly of meta-siltstone with locally dominant meta-limestone beds. We correlate these rocks to the well-studied Paleozoic rocks in the nearby El Paso Mountains (Dibblee, 1952; Carr et al., 1997). Distinctive units within this sequence allow a stratigraphic correlation to rocks in the eastern El Paso Mountains (Fig. 2); the details of this correlation are described further in the fault slip section.

#### Mesozoic Plutonic and Metamorphic Rocks

A few small bodies of chlorite-altered quartz diorite intrude metasedimentary rocks in the Christmas Canyon area. These rocks have similar mineralogy, textures, and alteration as the Jurassic Laurel Mountain pluton (Carr et al., 1997) that intrudes correlative metasedimentary

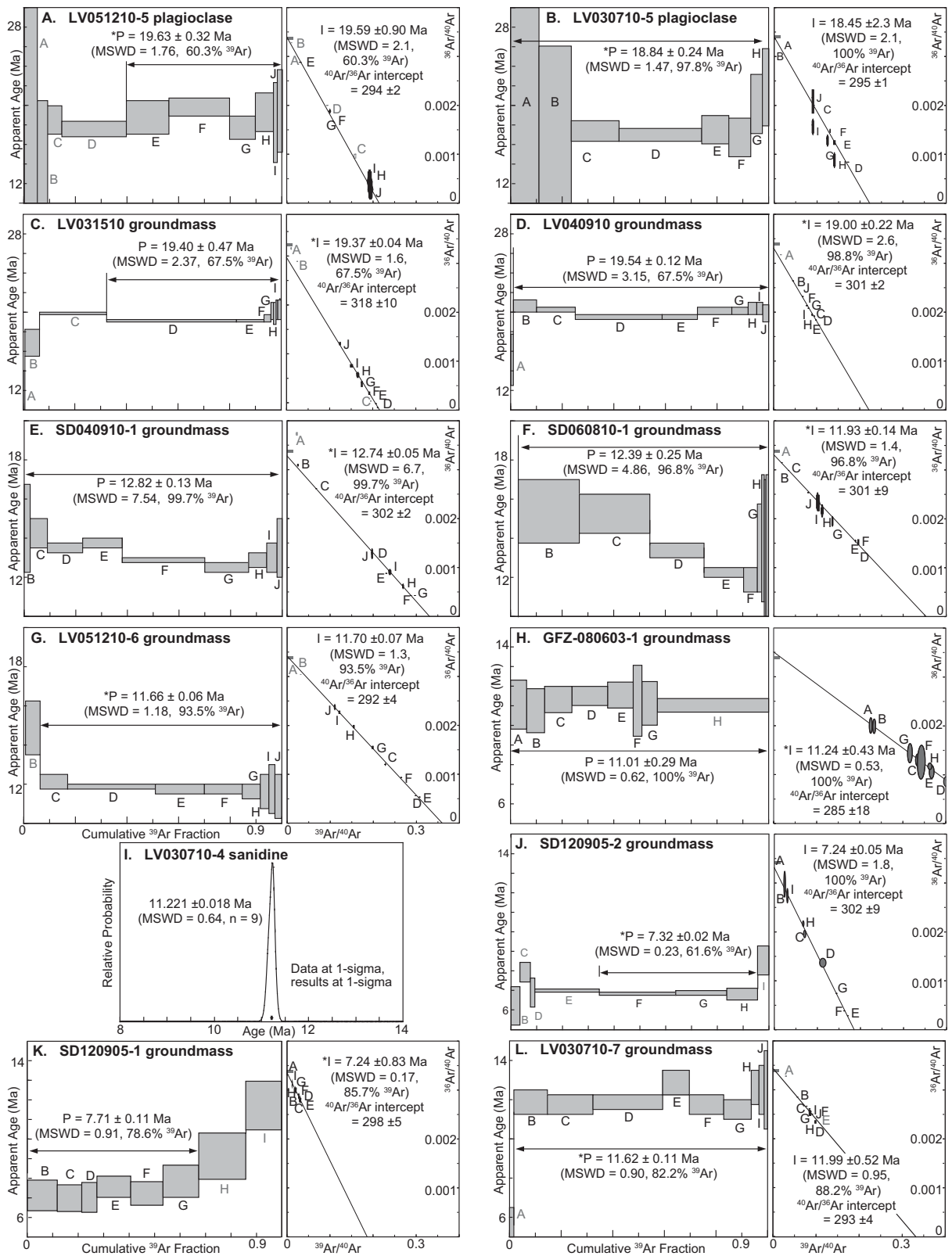


**Figure 4.** Plots of plateau diagrams and inverse isochrons for step-heating <sup>40</sup>Ar/<sup>39</sup>Ar analyses of our new samples, except I, which is a frequency plot of analyses of sanidine (MSWD—mean square of weighted deviates). Interpreted ages are reported using plateau (P) and inverse isochron (I) methods with the preferred age denoted by (\*). Double-headed arrows indicate the steps included in the plateau age. Fraction labels (i.e., A, B, C, etc.) in gray were not used in the age interpretation. The small gray box on the inverse isochron plots denotes the value of atmospheric argon with <sup>40</sup>Ar/<sup>36</sup>Ar of 295.5.

TABLE 2.  $^{40}\text{Ar}/^{39}\text{Ar}$  GEOCHRONOLOGY INTERPRETATIONSA. New  $^{40}\text{Ar}/^{39}\text{Ar}$  samples

- LV051210-5** (IGSN:JEA0522MM). Sample of basaltic andesite from below dacite lava in the Lava Mountains. Plagioclase from this sample shows a complicated plateau pattern (Fig. 4A), but the large errors allow a valid plateau with an acceptable mean standard weighted deviates (MSWD). Inverse isochron analysis gives a similar age with a slightly higher MSWD. The preferred age is  $19.63 \pm 0.32$  Ma from the plateau diagram. The age and stratigraphic position of this lava fits with a correlation to the Eagle Crags Volcanics (Sabin, 1994; Monastero et al., 1997).
- LV030710-5** (IGSN:JEA0522M7). Sample of basaltic andesite from below dacite lava. Plagioclase from this sample has a saddle-shaped plateau (Fig. 4B) but yields a plateau of  $18.84 \pm 0.24$  Ma with an acceptable MSWD. The inverse isochron has higher errors and MSWD. The age and stratigraphic position of this lava fit with a correlation to the Eagle Crags Volcanics (Sabin, 1994; Monastero et al., 1997).
- LV031510** (IGSN:JEA0522MB). Sample of dacite clast from silicified breccia deposit from below dacite lava in the Lava Mountains. Groundmass from this sample has a slight saddle-shaped plateau (Fig. 4C) that gives a relatively high MSWD. Inverse isochron analysis yields a better MSWD value with a slightly higher  $^{40}\text{Ar}/^{39}\text{Ar}$  intercept value than the atmosphere. The inverse isochron age of  $19.37 \pm 0.04$  Ma is the preferred age. The age and stratigraphic position of this lava fit with a correlation to the Eagle Crags Volcanics (Sabin, 1994; Monastero et al., 1997).
- LV040910** (IGSN:JEA0522MD). Sample of dacite clast from silicified breccia deposit from below dacite lava in the Lava Mountains. Groundmass from this sample has a saddle-shaped plateau (Fig. 4D) that gives a relatively high MSWD. Inverse isochron analysis yields a better but still high MSWD value and a slightly higher  $^{40}\text{Ar}/^{39}\text{Ar}$  intercept value. The inverse isochron age of  $19.00 \pm 0.22$  Ma is the preferred age. The age and stratigraphic position of this lava fit with a correlation to the Eagle Crags Volcanics (Sabin, 1994; Monastero et al., 1997).
- SD040910-1** (IGSN:JEA0522MU). Sample of basalt lava below dacite lava. Groundmass from this sample has a disturbed plateau with decreasing age (Fig. 4E) similar to sample SD060810-1. Inverse isochron plot gives an age of  $12.74 \pm 0.05$  Ma with a slightly better fit but has a high MSWD of 6.7 and a slightly high value for atmospheric argon. We interpret the plateau pattern as excess argon and therefore this interpreted age is a maximum age. This interpretation fits with the slightly younger ages (11.66 and 11.93 Ma) of other basalts in the base of the Summit Range volcanics.
- SD060810-1** (IGSN:JEA0522MT). Sample of basalt lava from the Summit Range, below dacite lava. Groundmass from this sample has a disturbed plateau with progressive steps with decreasing ages (Fig. 4F) that shows two ages at ca. 15 Ma and ca. 12 Ma. Inverse isochron plot gives a better fit with a MSWD of 1.4. The anomalous older age steps may be the result of alteration or maybe contamination by slightly older igneous rocks. The preferred age is  $11.93 \pm 0.14$  Ma, which fits with the age range of other basalts in the base of the Summit Range volcanics.
- LV051210-6** (IGSN:JEA0522MK). Sample of the basal basalt lava flow in the Black Hills over tuff deposits and basaltic-andesite flows. Groundmass from this sample yields a valid plateau age of  $11.66 \pm 0.06$  Ma (Fig. 4G) with a reasonable MSWD value, and inverse isochron gives a similar age and slightly higher MSWD. This age fits with the ages of other basalts in the base of the Summit Range Volcanics.
- GFZ-080603-1** (IGSN:JEA052263). Sample of orthoclase megacrystic dacite lava that is part of the Summit Range volcanics. Biotite from this sample has an odd plateau behavior (Fig. 4H) with a large-volume, high-temperature step with a lower age. A valid plateau for the entire step-heating yields  $11.01 \pm 0.29$  Ma with a MSWD of 0.62. The inverse isochron yields a similar age to the plateaus but with slightly better MSWD value. Therefore our preferred age is  $11.24 \pm 0.43$  Ma age from the inverse isochron. This age is the same, within error, as the other orthoclase megacrystic dacite (sample LV030710-4; Fig. 4I).
- LV030710-4** (IGSN:JEA0522M6). Sample of orthoclase megacrystic dacite lava that is part of the Summit Range volcanics. This sample was analyzed via total fusion of sanidine fractions (Fig. 4I). Frequency analysis of these data yields an age of  $11.221 \pm 0.018$  Ma.
- SD120905-2** (IGSN:JEA0522MS). Sample of vitrophyric dacitic intrusion with fine-grained (<1 mm) needles of hornblende. We correlate this unit to the Lava Mountain Dacite. Groundmass from this sample has a plateau age of  $7.32 \pm 0.02$  Ma with low MSWD (Fig. 4J). The inverse isochron yields a similar age but with a higher MSWD. This sample is similar in appearance to sample SD120905-1. This sample has odd plateau shape which may indicate a relatively young, but still significant excess argon component. We interpret this age to be too old; see text for discussion.
- SD120905-1** (IGSN:JEA0522MR). Sample of finely vitrophyric dacitic intrusion that we correlate to the Lava Mountain Dacite. Groundmass from this sample has an odd-shaped plateau (Fig. 4K). The lowest age step (B) is  $7.46 \pm 0.33$  Ma. The inverse isochron yields a good fit with a low MSWD and an age of  $7.24 \pm 0.83$  Ma. This sample is mineralogically and texturally similar to the nearby sample SD120905-2, which exhibits a better plateau behavior and has an age similar to the age of the lowest age step and inverse isochron of this sample. We interpret this age to be too old; see text for discussion.
- LV030710-7** (IGSN:JEA0522M5). Basalt clast sample from the conglomerate of Golden Valley. Groundmass from this sample has a plateau (Fig. 4L) that yields the preferred age of  $11.62 \pm 0.11$  Ma. Inverse isochron analysis (without step A) gives a slightly higher MSWD but an older age with more error. The age of this basalt matches with the basalts at the base of the Summit Range volcanics.
- B. Reinterpreted  $^{40}\text{Ar}/^{39}\text{Ar}$  samples from Smith et al. (2002)
- GFZ-85** (IGSN:JEA0522085). Sample of dacite lava in the Summit Range volcanics. Biotite for this sample has a plateau age of  $11.32 \pm 0.94$  Ma using steps E–G (Fig. 6A). This analysis has a large analytical error of 7.66%. The inverse isochron has a low MSWD, but large age error of 8.6 m.y.
- LM96-15** (IGSN:JEALM9615). Sample of dacite lava in the Summit Range volcanics. Biotite from this sample has a plateau age of  $10.66 \pm 0.12$  Ma (Fig. 6B) but a high MSWD because the three plateau steps define a slope. The inverse isochron has a higher MSWD.
- LM96-16** (IGSN:JEALM9616). Sample of dacitic volcanic debris-flow deposit in the Almond Mountain Volcanics. Biotite from this sample yields a valid plateau age of  $7.82 \pm 0.22$  Ma (Fig. 6C). The plateau diagram has a saddle shape, so this age may include an excess argon component and therefore this interpreted age may be too old. The inverse isochron has a similar age with many anomalous fractions and a slightly high  $^{36}\text{Ar}/^{39}\text{Ar}$  value. Hornblende does not yield a valid plateau (Fig. 6D) because of step K, which released 79% of the  $^{39}\text{Ar}$ . Step K has an age of  $8.65 \pm 0.67$  Ma, just barely overlapping, within error, with the biotite plateau. The hornblende inverse isochron yields a ca. 7 Ma age, but with an anomalous  $^{36}\text{Ar}/^{40}\text{Ar}$ .
- LM96-2** (IGSN:JEALM9602). Sample of dacitic sill. Biotite data do not yield a valid plateau (Fig. 6E), but steps F and G are 74.5% of the  $^{39}\text{Ar}$  released. Steps F and G yield the preferred age for this rock of  $7.64 \pm 0.18$ . The biotite inverse isochron gives a similar age but has a large MSWD. The hornblende for this sample yields valid plateaus (Fig. 6F) and isochron ages of ca. 10 Ma, but has  $\sim 10\%$  age error and is  $\sim 2.7$  m.y. older. We interpret the hornblende to have an inherited component. We correlate this intrusive unit with the Lava Mountains Dacite, based on its location and that it cuts the Almond Mountain Volcanics.
- LM96-17** (IGSN:JEALM9617). Sample of tuff in Almond Mountain Volcanics interbedded with Bedrock Spring Formation. Hornblende from this sample does not yield a valid plateau (Fig. 6G). A three-point isochron yields an age of  $9.98 \pm 0.09$  Ma with a large MSWD and a large  $^{40}\text{Ar}/^{36}\text{Ar}$  error. This analysis does not yield a valid age.
- LM1132** (IGSN:JEALM1132). Sample from thick gray dacite lava flow. Biotite from this sample does not define a valid plateau or inverse isochron (Fig. 6H). This analysis does not yield a valid age.

Note: Additional data for these samples are included in Tables DR1 and DR3 (see text footnote 1) and also accessible at <http://www.geosamples.org/> using the International Geo Sample Number (IGSN).



TABLE 3. U/Pb ZIRCON GEOCHRONOLOGY RESULTS

Sample name	IGSN*	Unit code <sup>†</sup>	Geologic context	Age (Ma)	Age error (± Ma)	MSWD <sup>§</sup>	n
LV050810-4	JEA0522MI	LMD	Dacite lava flow	6.507	0.070	1.9	2
LV051810-8	JEA0522MO	LMD	Vitrophyric dacitic sill	6.522	0.026	2.8	3
JDW-20	JEA0522MQ	AMV	Thick pink tuff	7.479	0.023	3.5	4
LV050710	JEA0522MH	SRV	Upper dacite lava flow/dome	10.490	0.054	1.2	5
LV031410-B	JEA0522MA	SRV	Lower dacite lava dome	10.966	0.042	2.4	5
CINCO	JEACINCO1	SRV	Megacrystic dacitic dike	11.383	0.028	1.2	6

Note: Additional data for these samples are included in Table DR2 (see text footnote 1).

\*International Geo Sample Number data accessible at <http://www.geosamples.org/>.

<sup>†</sup>Unit Code: Stratigraphic unit that the sample belongs to: ECV—Eagle Crag Volcanics; SRV—Summit Range volcanics; AMV—Almond Mountain Volcanics; LMD—Lava Mountain Dacite.

<sup>§</sup>MSWD—mean standard weighted deviates.

rocks in the eastern El Paso Mountains (Fig. 2). A few small exposures of similar quartz diorite occur in the northeastern Summit Range adjacent to the Garlock fault (Fig. 2). All of the other basement in the LMSR is quartz monzonite to granodiorite of the Cretaceous Atolia Quartz Monzonite (Hulin, 1925; Smith, 1964).

### Cenozoic Units

**Lower Miocene volcanic-sedimentary rocks.** The oldest Cenozoic units in the LMSR are widespread but discontinuous felsic ash and pumice lapilli tuffs (Figs. 3 and 7). These tuffs are white, distinctively bedded with beds 5–15 cm thick, and have local interbeds of arkosic sandstone. The tuffs are overlain by oxidized porphyritic basaltic-andesite to andesite lava and are intruded by intermediate-composition porphyry (Dibblee, 1967). The lavas have  $^{40}\text{Ar}/^{39}\text{Ar}$  ages of  $19.63 \pm 0.32$  Ma on plagioclase (Fig. 4A) and  $18.84 \pm 0.24$  Ma on plagioclase concentrate (Fig. 4B). Silicified volcanic breccia deposits overlie the tuffs in the Christmas Canyon area. The clasts are dark colored and aphyric, and are dacites based on geochemical analyses (Monastero, unpub. data). These rocks have  $^{40}\text{Ar}/^{39}\text{Ar}$  ages of  $19.37 \pm 0.04$  Ma on groundmass (Fig. 4C) and  $19.00 \pm 0.22$  Ma on groundmass concentrate (Fig. 4D), similar to ages of the altered lava flows (Table 2). We correlate these rocks to the Eagle Crag Volcanics, based on age, composition, and stratigraphic relations (Sabin, 1994). Monastero et al. (1997) correlated the Eagle Crag Volcanics to the Cudahy Camp Formation (Cox and Diggles, 1986) in the El Paso Mountains.

**Middle Miocene basalt.** Vesicular basalt overlies the lower Miocene units in the LMSR. These are finely porphyritic with olivine and pyroxene and occur as 2–4-m-thick flows in the Summit Range and Lava Mountains but as a 25-m-thick sequence in the Black Hills. Basalts in the Summit Range and Lava Mountains have  $^{40}\text{Ar}/^{39}\text{Ar}$  groundmass ages of  $<12.74 \pm 0.05$  Ma (Fig. 4E; Table 2) and  $11.93 \pm 0.14$  (Fig. 4F), and the oldest basalt in the Black Hills has an age of  $11.66 \pm 0.06$  Ma (Fig. 4G).

### Upper Miocene Summit Range Volcanics.

The basalts and older units in the Summit Range and Lava Mountains are overlain by a few-meters-thick conglomerate containing rounded and polished cobble- to boulder-sized clasts of felsic plutonic rocks and also of distinctive flow-banded rhyolite. A sequence of volcanic rocks occurs above beginning with a several-meters-thick tuff containing plutonic lithic blocks, pumice lapilli, and numerous lenses of dacitic lava breccia. These units are overlain by and interbedded with several bodies of dacite lava that have textures ranging from aphyric to porphyritic to megacrystic porphyritic. The dacite lava flows are thick (50–150 m), have limited areal extent (less than 1000 m long), and have the stratigraphic expression and textures of dacitic lava domes (Andrew et al., 2014). Feldspar and biotite porphyritic dacite lavas have  $^{40}\text{Ar}/^{39}\text{Ar}$  ages of  $11.32 \pm 0.94$  Ma (Fig. 6A) and  $10.66 \pm 0.12$  Ma (Fig. 6B) on biotite and U-Pb zircon ages of  $10.966 \pm 0.042$  Ma (Fig. 5A; Table 3) and  $10.490 \pm 0.054$  Ma (Fig. 5B). Quartz-biotite-feldspar porphyritic dacite lavas containing distinctive 1–4 cm megacrysts of orthoclase have  $^{40}\text{Ar}/^{39}\text{Ar}$  ages of  $11.24 \pm 0.43$  Ma on groundmass concentrates (Fig. 4H) and  $11.221 \pm 0.018$  Ma on sanidine (Fig. 4I). We modify terminology of Smith et al. (2002) and refer to these dacite dome complexes of lava, tuff, and epiclastic deposits as the Summit Range volcanics (Fig. 3).

### Upper Miocene Bedrock Spring Formation–Almond Mountain Volcanics.

Arkosic sandstone of the Bedrock Spring Formation (Smith, 1964) unconformably overlies the dome complexes and older rocks in the Lava Mountains, Summit Range, and Christmas Canyon area. The basal unconformity with the dacite domes varies from disconformity to angular unconformity to buttress unconformity. Thin lenses (generally <15 cm) of pebble to cobble conglomerate occur throughout the section, as do locally abundant layers of siltstone. Limestone beds and well-cemented arkose occur only along the south sides of the dacite lava domes. These are likely lacustrine deposits resulting from pond-

ing upstream of the dacite domes. Sediment transport in the Bedrock Spring Formation was to the northwest (Smith, 1964; this study), so the domes would have formed topographic barriers.

Dacitic volcanic deposits of the Almond Mountain Volcanics overlie and are intercalated with the upper parts of the Bedrock Spring Formation. These have pronounced facies changes across the LMSR, ranging from 200-m-thick complexes of multiple units (Fig. 8A) to sections with only a single pumice lapilli tuff bed (Fig. 8B). The thickest sequences occur in the southern Lava Mountains, with multiple volcanic debris-flow deposits of clasts of light-purple porphyritic dacite lava interbedded with several 2–10-m-thick pumice lapilli to lithic tuff beds and local sandstone beds. In the northeastern Lava Mountains, volcanic interbeds are mostly absent in the Bedrock Spring Formation except for one ~15-cm-thick pumice lapilli tuff and a 2-m-thick bed of dacitic volcanic debris-flow deposit. The Almond Mountain Volcanics are not present in the Black Hills area and are rare elsewhere in the LMSR; a 10-m-thick bed of tuff is exposed in the western Summit Range area and a 10–15-cm-thick tuff bed occurs in the upper parts of arkosic beds in the Christmas Canyon area. Dacitic lava above the Bedrock Spring Formation has a  $^{40}\text{Ar}/^{39}\text{Ar}$  of  $<7.82 \pm 0.22$  Ma on biotite (Fig. 6C; Table 2), and a tuff in the upper Bedrock Spring Formation has a U-Pb zircon age of  $7.479 \pm 0.023$  Ma (Fig. 5C).

**Upper Miocene Lava Mountains Dacite.** A thick porphyritic lava flow overlies the Bedrock Spring Formation and Almond Mountain Volcanics. Smith (1964) defined this as the “Lava Mountain Andesite”, but geochemical data (Smith et al., 2002) show that it is a dacite; therefore we propose the name “Lava Mountain Dacite”. This lava is a distinctive brownish gray and has porphyritic plagioclase, hornblende, and biotite with rare quartz and smaller and less-abundant pyroxene. It contains variable amounts of mafic clots a few centimeters in diameter. The unit is voluminous, covering >50 km<sup>2</sup> and 40–100 m thick. A sample from the Lava Mountain Dacite has a U-Pb zircon age of  $6.507 \pm 0.070$  Ma (Fig. 5D).

Another porphyritic dacite lava flow occurs just beyond the northern exposures of Lava Mountain Dacite. This flow is distinguished from the Lava Mountain Dacite in that it has a red color, pilotaxitic textures, and a 10–20-m-thick basal vitrophyre. We associate this flow with the Lava Mountain Dacite based on its similar phenocryst assemblage, thickness, location, and stratigraphic relationships. Smith (1964) also included this with his Lava Mountains Andesite.

Numerous vitrophyric sills intrude the Bedrock Spring Formation and Almond Mountain

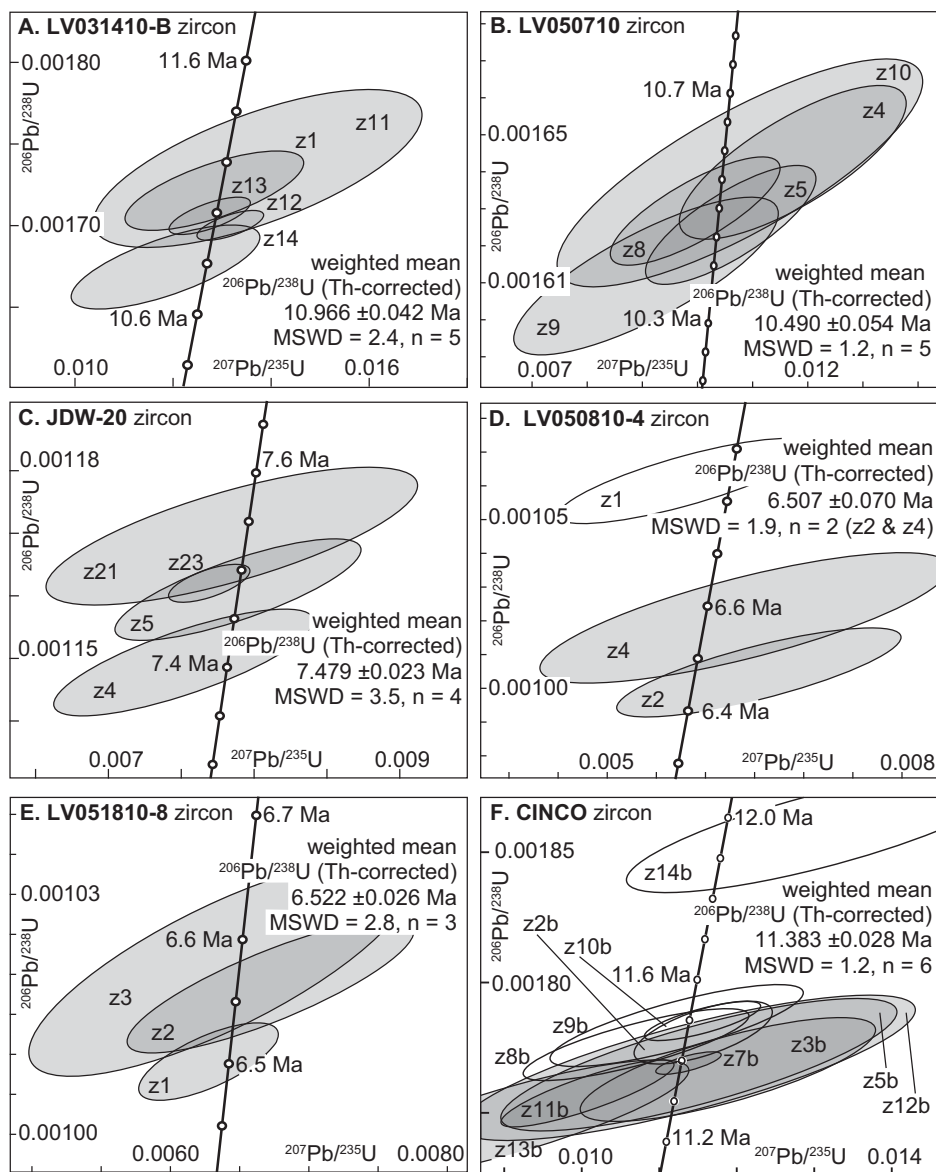


**Figure 5.** Concordia plots of U-Pb analyses of samples (MSWD—mean square of weighted deviates). Unfilled fraction error ellipses were not used to calculate the crystallization age.

Volcanics. Smith (1964) misinterpreted the intrusive front of one of these dacite sills (Fig. 8C) as a lava flow front of a “Quaternary andesite”. This roll structure is intrusive: there is no basal flow breccia and the contacts on all sides are baked. We correlate these sills with the Lava Mountain Dacite based on similar phenocryst mineralogy, location, and large volume, and because they cut the Almond Mountain Volcanics. These intrusives form a WNW-trending zone along the northern exposures of the Lava Mountain Dacite (Fig. 2). The red pilotaxitic lava occurs only along this zone of intrusions and may therefore be the near-vent facies of the Lava Mountain Dacite. Two other intrusive bod-

ies, in the western Summit Range (Fig. 2), are correlated to the Lava Mountain Dacite based on their vitrophyric texture and relationships to stratigraphic units. These have fine needles of hornblende and intrude the Bedrock Spring Formation and Almond Mountain Volcanics. Dibblee (1967) mapped these intrusions as basalt, but geochemical analyses show them to be dacitic (Monastero, unpub. data).

A vitrophyric sill from the central Lava Mountains area has a U-Pb zircon age of  $6.522 \pm 0.026$  Ma (Fig. 5E), but the biotite  $^{40}\text{Ar}/^{39}\text{Ar}$  age of a similar sill is  $7.64 \pm 0.18$  Ma (Fig. 6E; Table 2). The hornblende vitrophyric dacitic intrusions from the Summit Range have  $^{40}\text{Ar}/^{39}\text{Ar}$  ages of

$7.32 \pm 0.02$  Ma (Fig. 4J) and  $7.24 \pm 0.83$  Ma (Fig. 4K) on groundmass concentrates (Table 2). We postulate that the discrepancy between the U-Pb and  $^{40}\text{Ar}/^{39}\text{Ar}$  ages could reflect (1) an excess argon component, creating anomalously older ages, or (2) that the sills dated by  $^{40}\text{Ar}/^{39}\text{Ar}$  better correlate to the Almond Mountain Volcanics. The former is more likely because of the excess argon—interpreted hornblende  $^{40}\text{Ar}/^{39}\text{Ar}$  ages, which are older than those of biotite from samples of Almond Mountain Volcanics and from one of these sills (Fig. 6C and 6E).

**Plio-Pleistocene conglomerates.** Pebble to boulder conglomerates overlie the Miocene units in the LMSR area. These rocks contain no known datable units, but we infer them to be Pliocene based on their deposition over the Lava Mountain Dacite and their angular unconformable contacts with overlying Quaternary units. We break out two different sets of these conglomerates based on location and differences in clast types. Both units contain clasts of metasedimentary, meta-plutonic, plutonic, and volcanic rocks exotic to the LMSR, and also contain placer gold deposits (Dibblee, 1967; Fife et al., 1988). Boulders and cobbles of felsic plutonic rocks, felsic hypabyssal intrusive rocks, and quartzite are conspicuously well rounded and polished.

The informally defined conglomerate of Golden Valley is the eastern unit, which has distinctive lineated and foliated hornblende diorite clasts with a capping unit of boulders of vesicular basalt. These clast types distinguish it from the informally defined conglomerate of Hardcash Gulch in the Summit Range (Fig. 2), 15 km to the west. Rittase (2012) reported a tephrochronology age of 3.14 Ma for a tuff overlying exotic-clast conglomerates a few kilometers east of Christmas Canyon. A sample from a basalt boulder of the conglomerate of Golden Valley has a  $^{40}\text{Ar}/^{39}\text{Ar}$  age of  $11.62 \pm 0.11$  Ma (Fig. 4L), matching the age of the texturally and mineralogically similar basalt in the Black Hills.

## STRUCTURES

Previous studies of the LMSR show that the Cenozoic units are deformed (Smith, 1964; Dibblee, 1967; Smith et al., 2002) but did not determine kinematics of fault slip. New geologic mapping (Andrew et al., 2014) better defines these faults, identifies several new faults (Fig. 2), and identifies many stratigraphic markers to use in determining fault offset. Slip direction and sense of shear given for each fault below was determined by combining measurements of fault striations with two or more shear-sense indicators such as Riedel shears, fault gouge foliation, drag folding, fault-zone clast rotation, slickenfibers, asperity tool marks, and small-scale offset



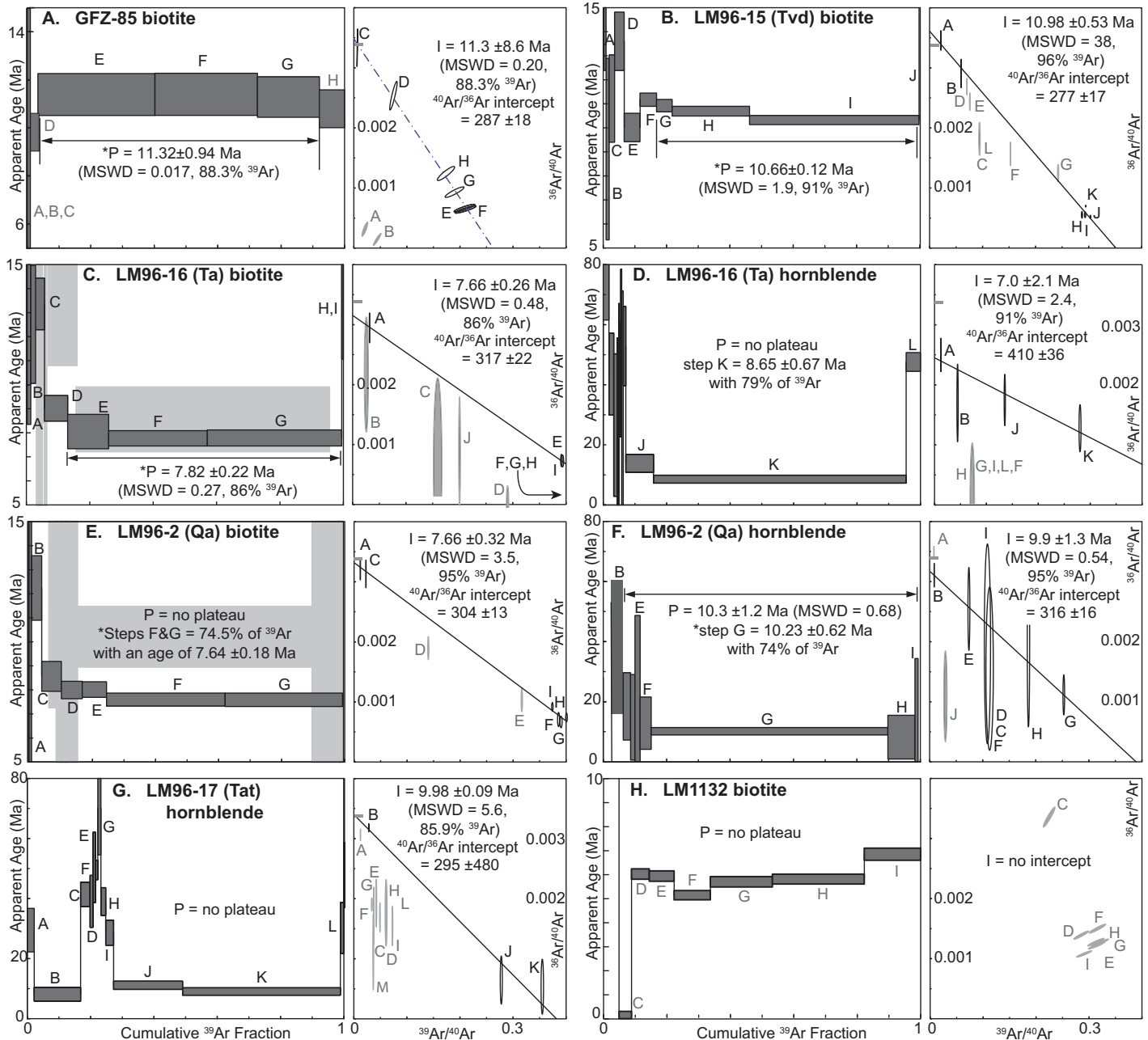


**Figure 6.** Plots of plateau diagrams and inverse isochrons for step-heating <sup>40</sup>Ar/<sup>39</sup>Ar analyses of the reinterpreted samples from Smith et al. (2002). See Figure 4 for symbol and abbreviation explanations. The gray blocks on C and E are the corresponding hornblende data for each sample.

(Tchalenko, 1970; Chester and Logan, 1987; Means, 1987; Petit, 1987). We also discuss folds of late Cenozoic units in the LMSR.

**Geometry and Kinematics of Faults**

**Sinistral Faults**

**Garlock fault.** Data for the Garlock fault in the western LMSR show left-lateral slip with low rake and an associated set of normal-slip fault

planes (Fig. 9A). Fault scarps of the Garlock fault in Quaternary alluvium (Rittase, 2012) show a similar orientation of fault planes (Fig. 9B).

**Teagle Wash fault.** The Teagle Wash fault (named herein) occurs in the northeast Summit Range (Fig. 2). It was previously interpreted as a thrust fault (Hulin, 1925; Smith, 1964) because it places granitic rock over Bedrock Spring Formation, Eagle Crags Volcanics, and green-altered medium-grained quartz diorite. This

quartz diorite is similar to intrusive rocks of the Jurassic Laurel Mountain granodiorite and not the more felsic and less altered Atolia Quartz Monzonite. Measured fault planes have low dips with low-rake fault striae (Fig. 9C). Top-to-the-ESE relative motion of this fault (Fig. 10A) equates to left-lateral oblique slip (Fig. 9C).

**Savoy fault.** The Savoy fault (named herein) separates the Summit Range from the Lava Mountains (Fig. 2). It has moderate dips to the

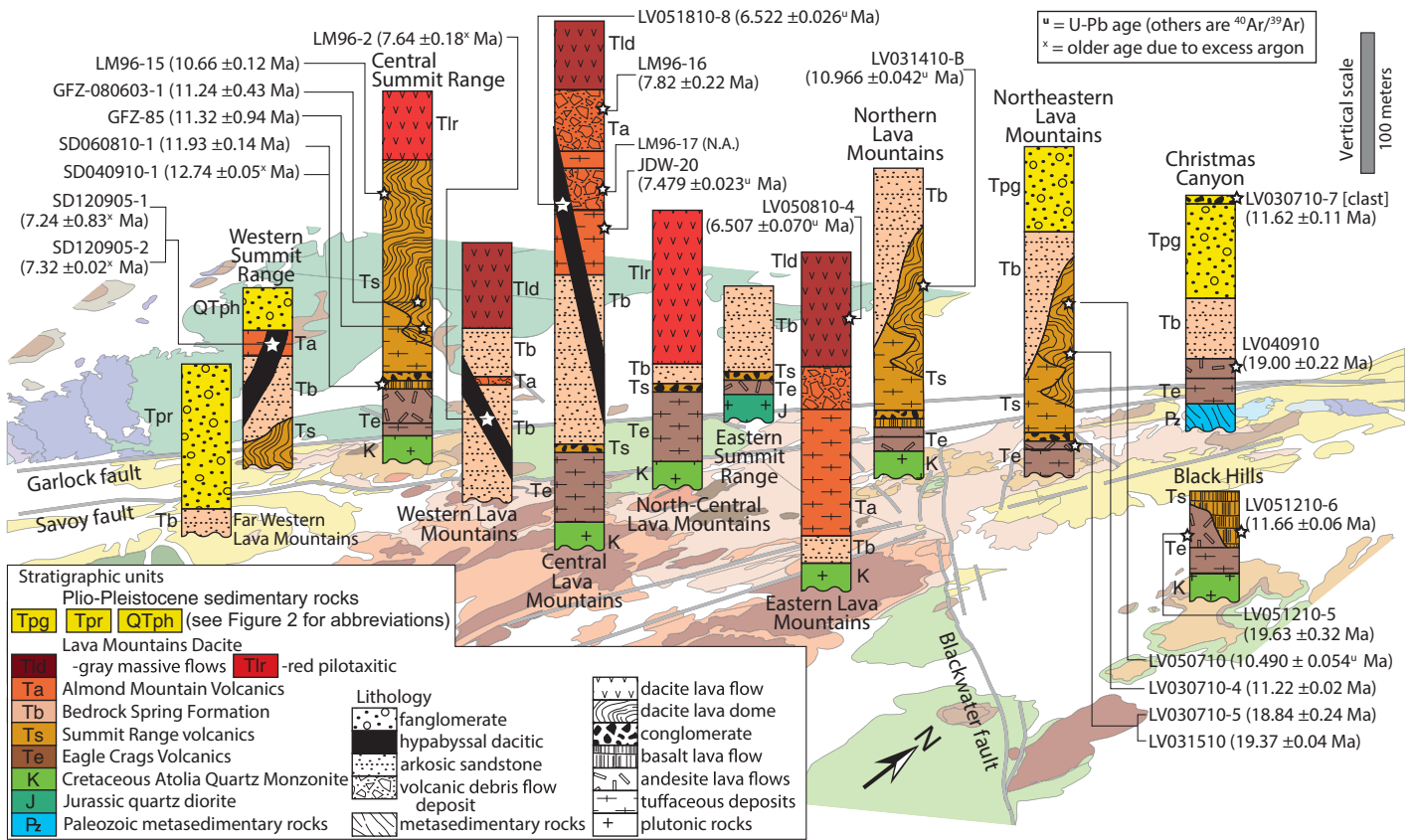


**Figure 7. Simplified stratigraphic columns across the Lava Mountains–Summit Range plotted on an oblique view of the same area as Figure 2. The lithology of each unit is denoted by fill patterns, and the stratigraphic unit is denoted by fill color and an adjacent unit label. Geochronological sample locations are denoted by stars with sample name and interpreted age in parentheses. Note that most of the contacts are unconformable and drawn only schematically.**

south, low-rake slip vectors (Figs. 9D, 10B, and 10C), and left-lateral sense of shear. The Savoy fault merges into the Garlock fault in the eastern LMSR. The Savoy fault continues westward into Quaternary fault scarps of the Cantil fault (Dibblee, 1952, 1967) and may be a continuation of the main trace of the western Garlock fault (WGF on Fig. 1).

**Browns Ranch fault zone.** The ~2-km-wide Brown’s Ranch fault zone has similar fault measurements and kinematics (Fig. 9E) to the Garlock fault (Fig. 9A). Exposures of the Brown’s Ranch fault zone show a multi-stranded structure with spatially associated folding of all of the Miocene units with axes roughly parallel to the strike of this fault zone (Fig. 10D).

**Oblique Fault**

**Little Bird Fault.** The boundary between the Paleozoic basement of the Christmas Canyon area and the Atolia Quartz Monzonite basement present in the rest of the LMSR is a WNW-striking fault that juxtaposes lower Miocene rocks against Bedrock Spring Formation. Limited fault measurements along this and subsidiary

faults indicate sinistral-oblique thrust kinematics (Fig. 9F). We refer to this as the Little Bird fault (Fig. 2). The fault is unconformably overlapped by the conglomerate of Golden Valley.

**Normal Fault**

**Randsburg Wash fault zone.** To the east of the Blackwater fault, Smith (1964) and Oskin and Iriondo (2004) mapped a zone of faults oriented similar to the Brown’s Ranch fault zone. This fault zone is poorly exposed, but limited data show northeast-striking faults with dip-slip motion (Fig. 9G) dissimilar to that of the oblique strike-slip Brown’s Ranch fault zone. We consider it to be a different structure and name it the Randsburg Wash fault zone (RWFZ on Fig. 2). These faults are inferred to have slip as young as late Pleistocene based on along-strike fault scarps 12 km to the east that Smith et al. (1968) interpreted as late Pleistocene features.

**Dextral Fault**

**Blackwater fault.** The Blackwater fault juxtaposes Quaternary alluvium against Cretaceous granitic and Miocene rocks (Fig. 2). This fault

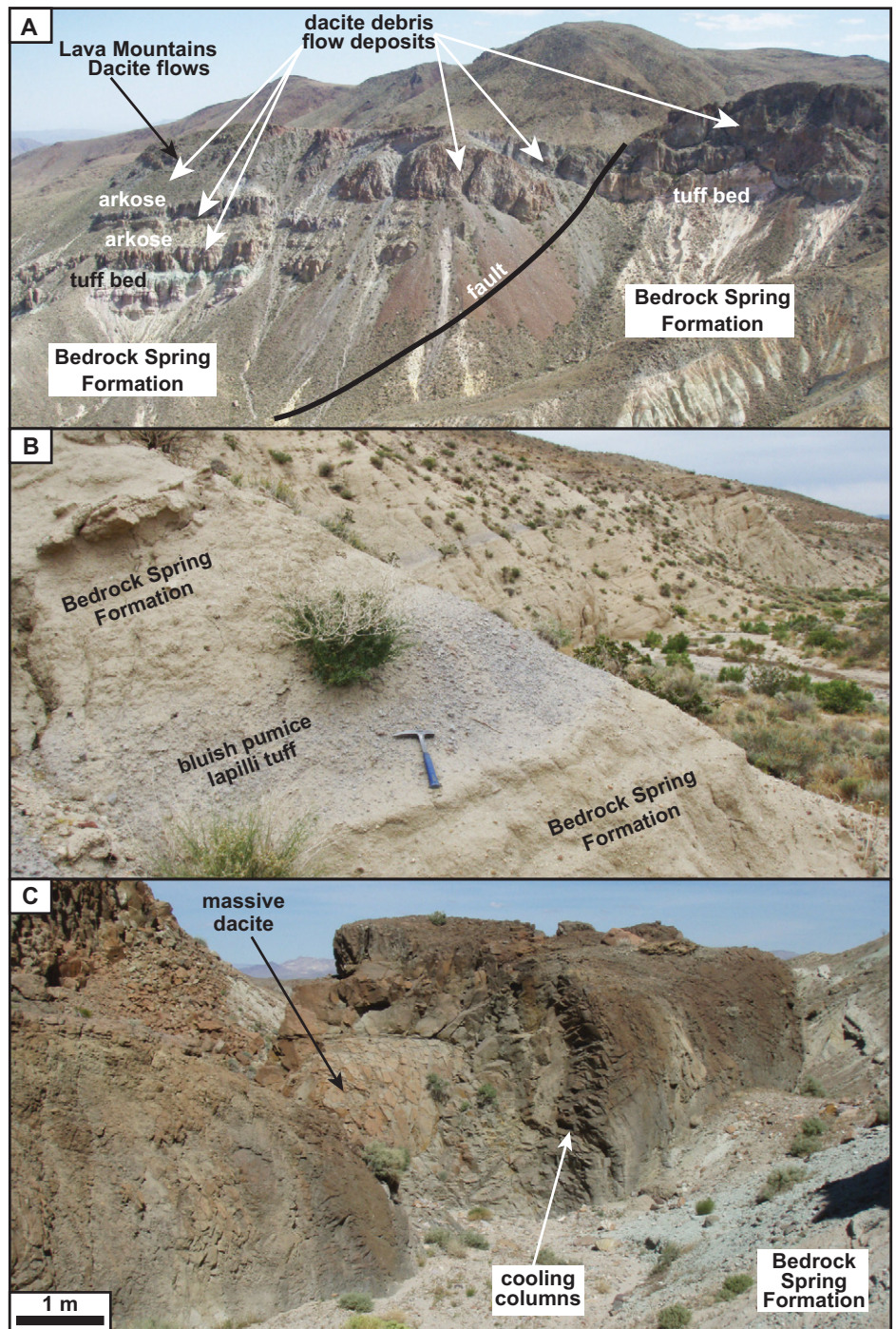
strikes NNW-SSE, dips steeply, has low-rake fault striae (Fig. 9H), and has dextral motion. The Blackwater fault continues northward past the Brown’s Ranch fault zone (Andrew et al., 2014), in contrast to the interpretation of Oskin and Iriondo (2004) that it to loses slip before this point. The northward continuation has a slightly different geometry, with a more northwesterly strike, lower dips, and right-oblique normal slip (Fig. 9I). There are also sets of normal and thrust faults associated with the northern part of this fault (Fig. 9I).

**Folds**

Smith (1964) identified folds in the Lava Mountains that deform upper Miocene units about WSW-trending fold axes (Fig. 9J). These folds form anticline-syncline pairs in the Bedrock Spring Formation that have steeply overturned SSE-facing central limbs. Miocene bedding also show a second possible fold orientation that plunges shallowly to the NNW (Fig. 9J). Bedding for Miocene units in the Christmas Canyon area are interpreted to have both of these



**Figure 8.** Photographs of select late Miocene geologic units in the Lava Mountains–Summit Range. (A) View of thickest section of Almond Mountain Volcanics. Scale varies; the steep cliff face is ~200 m tall. (B) View of the distal volcanic facies of the Almond Mountain Volcanics, where it occurs as a single thin tuff bed. Hammer (33 cm long) for scale. (C) View of roll structure of dacite that Smith (1964) interpreted as a lava flow edge, but which is the lateral edge of a shallow-level intrusion.



fold sets, although the WSW-trending set is less tightly folded (Fig. 9K). The younger conglomerate of Golden Valley is folded only about the WSW-trending fold axes (Fig. 9L). The lack of the NNW-trending fold set in this Pliocene unit indicates that the NNW-trending folds occurred prior its deposition.

**Magnitude and Rates of Fault Slip**

Following the example of Andrew and Walker (2009), we identified as many markers as possible in order to obtain maximum resolution on the amount and timing of motions of individual fault systems (see Table 4 for details and methods for determining uncertainty). The above section on fault geometry and kinematics shows that the major faults in the LMSR, except for the Randsburg Wash fault zone, are dominantly strike-slip faults; therefore we can approximate the fault slip as horizontal offsets in map view. The interpreted slip markers discussed below are shown mostly on Figure 11 with a few regional markers on Figure 1. These markers vary from blunt area restoration markers to relatively precise narrow linear feature restorations. Slip rates are calculated for all of the faults (Table 4) but are discussed only for the Garlock fault.

**Sinistral Faults**

**Garlock fault—Christmas Canyon area.** We interpret that the Christmas Canyon basement rocks correlate to rocks in the eastern El Paso Mountains using distinctive Paleozoic metasedimentary units that are appropriate to use as slip markers, because they are thin (60 ± 10 m), have steep dips, and strike roughly perpendicular to the Garlock fault. A quartzite–black slate bed (A on Fig. 11) matches a correlative bed in the eastern El Paso Mountains (A’ on Fig. 11). A meta-conglomerate layer (B on Fig. 11) matches a narrow zone of rocks in the eastern El Paso Mountains (B’ on Fig. 11), but it is less well exposed in the LMSR. Offset needed to restore

the quartzite-slate marker bed along the Garlock fault is 32.9 ± 0.6 km (Table 4). Larger slip is unlikely because metasedimentary rocks farther west in the El Paso Mountains have higher metamorphic grades, contain abundant metavolcanic rocks, and are intruded by ductilely deformed plutons (Dibblee, 1952; Carr et al., 1997).

We correlate a set of Pliocene rocks in the Christmas Canyon area to rocks in the eastern El Paso Mountains (Carter, 1994; Carr et al., 1997;

Smith et al., 2002); this correlation can be used to constrain slip on this segment of the Garlock fault. The Pliocene conglomerate of Golden Valley contains clasts exotic to the LMSR and placer gold (Fife et al., 1988). A subset of these clasts has distinctive well-rounded and polished textures: felsic plutonic, felsic hypabyssal, and quartzite. The exotic clasts, placer gold, and well-rounded clasts match to a sediment source in the El Paso Mountains: the Paleocene Goler



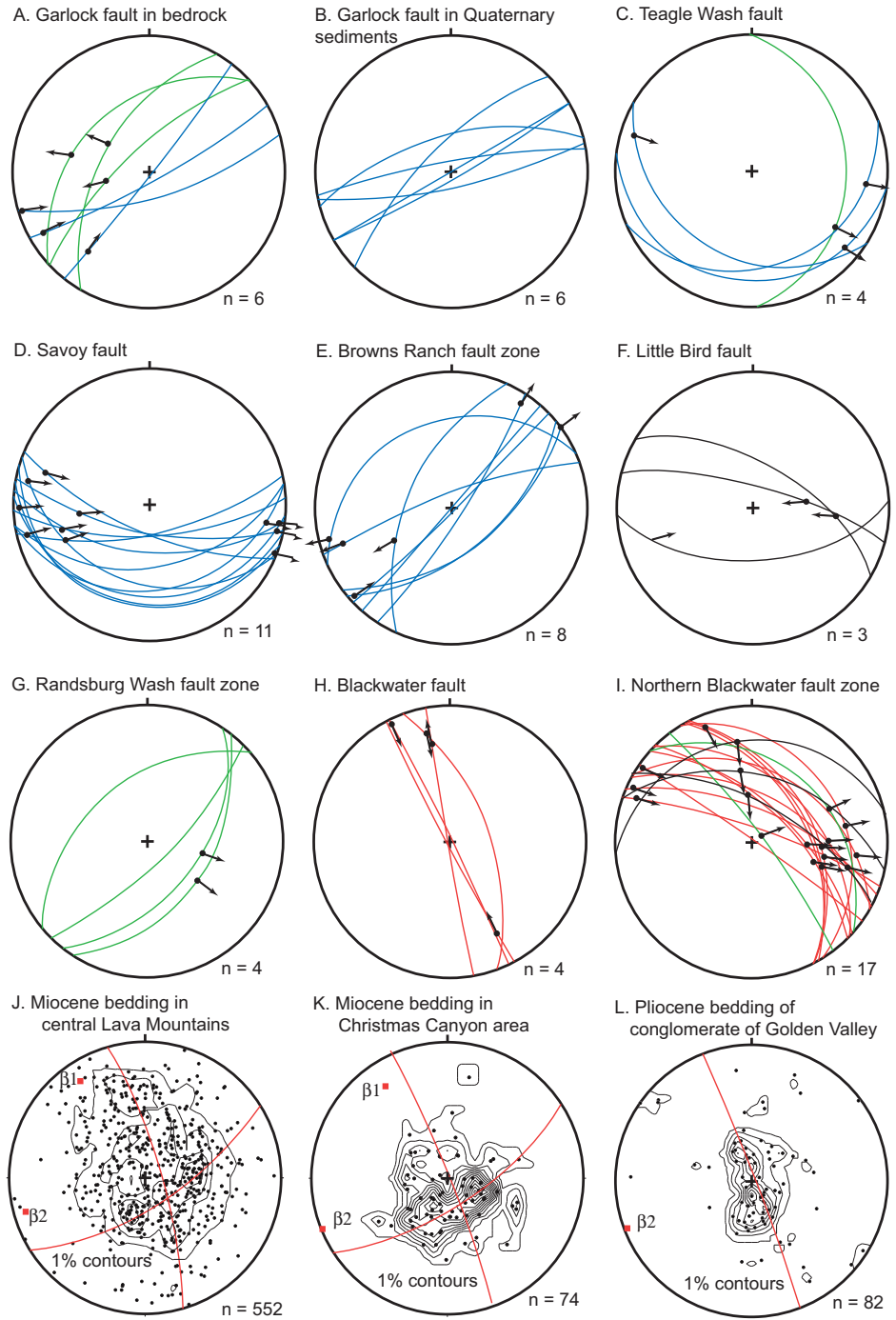


**Figure 9.** Stereographs of fault and bedding data for the Lava Mountains–Summit Range. Stereographs A–I plot data for the main fault plane for each major fault plus a few associated faults. Fault planes are great circles with the corresponding fault striae plotted as a point on the great circle. The motion of the hanging wall of each fault is indicated by the arrow away from the center. Faults are color-coded by dominant slip type: sinistral = blue, dextral = red, normal = green, and thrust = black. Stereographs J–L plot poles to bedding for different units with best-fit fold girdles in red and corresponding fold axes labeled  $\beta 1$  and  $\beta 2$ .

**Figure 10** (on following page). Photographs of faults in the Lava Mountains–Summit Range. Note the dot-in-circle and cross-in-circle symbols that represent motion out of and into the plane of view, respectively. (A) View of the Teagle Wash fault looking upward 30° from horizontal toward the southwest. This view is oblique to the fault striae. The fault juxtaposes Atolia Quartz Monzonite over Bedrock Spring Formation via left-lateral slip on a low- to moderate-angle fault (dipping away in this view). (B) Horizontal-looking view toward the south of the traces of two splays of the Savoy fault. Each splay has a few centimeters of gouge creating a horse of the Bedrock Springs Formation that is sheared and deformed in a left-lateral sense. (C) Detailed oblique view of the Savoy fault looking southwestward, at an angle to the strike. The kinematic indicators show normal oblique left-lateral slip. (D) Along-strike, northeast-looking, cross-sectional view of the Brown’s Ranch fault zone cutting volcanic debris-flow deposits of dacite and arkosic sandstone of the Bedrock Spring Formation. Note the associated syncline. (E) Detailed view of the northern Blackwater fault, looking toward the southeast, with kinematic indicators showing a normal component of oblique slip.



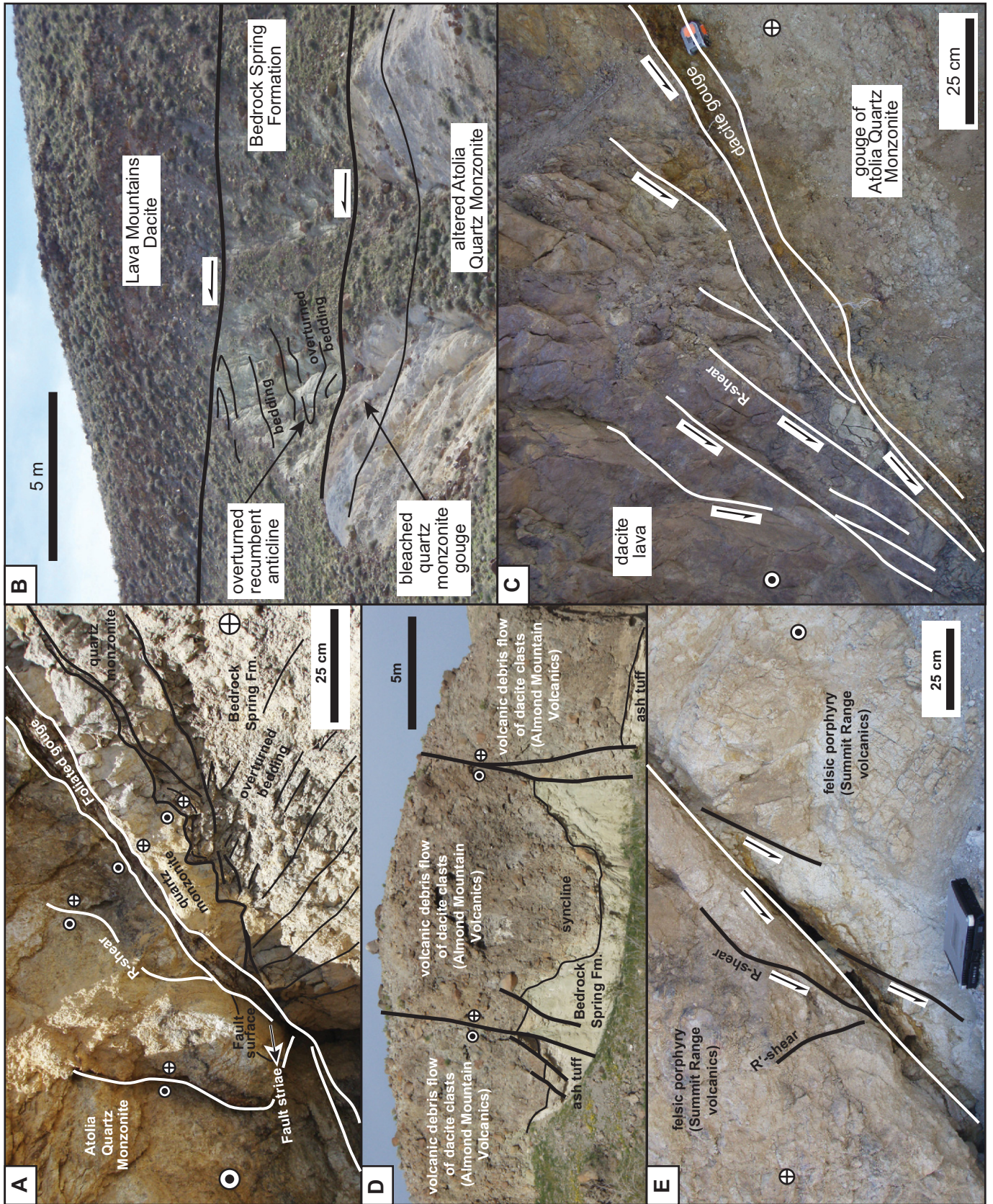


Figure 10.



Formation (Fig. 2). The basal Goler Formation contains coarse conglomerates derived from the El Paso Mountains and the Sierra Nevada Mesozoic batholith, quartzite clasts of unknown provenance (Cox, 1982), and placer gold (Dibblee, 1952). The farther-traveled clasts of the Goler Formation (felsic plutonic and quartzite) have well-rounded and polished textures (Cox, 1982). We rule out a bedrock source for the exotic clasts in the LMSR based on the intermixture of clast types, which are derived from bedrock sources in both the western and eastern ends of the El Paso Mountains, and the presence of clasts from the Sierra Nevada batholith and quartzite clasts.

Clasts of altered volcanic rock are also present in the conglomerate of Golden Valley. A possible source for these clasts is the Cudahy Camp Formation in the El Paso Mountains, which overlies the Goler Formation (Dibblee, 1952; Loomis and Burbank, 1988; Monastero et al., 1997). A potential specific source for all of these clasts is Goler Gulch (Fig. 2), which cuts through the Goler and Cudahy Camp Formations. Goler Gulch is the largest drainage system of the eastern El Paso Mountains and the only one to cut across the El Paso Mountains southern escarpment. We thus envision it to be a long-lived feature capable of supplying sediment to the southern El Paso Mountains where the Garlock fault would subsequently transport it away.

The clasts in the conglomerate of Golden Valley in the Christmas Canyon area (C on Fig. 11) are offset 30.2–39.2 km (Table 4) from Goler Gulch in the eastern El Paso Mountains (C' on Fig. 11). This offset of a wide-area feature agrees with the  $32.9 \pm 0.6$  km offset of the Paleozoic marker beds. This implies that slip on this segment of the Garlock fault initiated after deposition of the conglomerate of Golden Valley (6.5–3.14 Ma). Simple slip-rate calculations using these data yield long-term slip rates of 5.0–10.7 mm/yr (Table 4). These are similar to neotectonic slip rates for the central Garlock fault of 7–14 mm/yr (Rittase et al., 2014) and the slightly longer-term rate of 5–9 mm/yr (McGill and Sieh, 1993).

**Garlock fault—Summit Range.** The Atolia Quartz Monzonite in the Summit Range matches across the Garlock fault to similar rocks in the southeastern Sierra Nevada (Fig. 1; Saleeby et al., 2008). Garlock fault offset for restoring these rocks is poorly constrained to >42 km using the easternmost exposures of Cretaceous plutonic rocks in the Sierra Nevada (Fig. 1). A megacrystic dacite lava dome in the Summit Range is cut by the Garlock fault (D on Fig. 11), so it probably continued northward but there are no known dacite lavas on

TABLE 4. SLIP CONSTRAINTS FOR FAULTS IN LAVA MOUNTAINS–SUMMIT RANGE AREA

Label*	Slip constraint geologic feature		Correlated feature on opposite side of fault		Slip rate (mm/yr)	Age (Ma) <sup>b</sup> [error]	Notes
	Description	D <sup>1</sup> (km)	Description	D <sup>1</sup> (km)			
<b>Garlock fault along Christmas Canyon area</b>							
A	Quartzite and black slate beds in meta-siltstone and meta-limestone sequence**	0.91	A'	Quartzite and black slate of middle member of the metasedimentary rocks of El Paso Peaks (Carr et al., 1997)	32.9 [± 0.6]	ca. 460	This measurement includes a fault with ~800 m of left-lateral offset in the eastern El Paso Mountains (Carr et al., 1997)
B	Metaconglomerate in meta-siltstone sequence in Christmas Canyon area	1.85	B'	Metaconglomerate of the metasedimentary rocks of Holland Camp (Carr et al., 1997)	32.4 [± 0.8]	ca. 340	
C	Distinctive boulder clast assemblage in conglomerate of Golden Valley. Also rounded boulder textures and placer gold.	0.80	C'	Deposition across Garlock fault from Goler Gulch which cuts clast sources of Goler Formation and Cudahy Camp Formation. See text discussion.	34.7 [± 4.5]	3.14 to 6.5	This conglomerate is sourced from the eastern El Paso Mountains. Modern Goler Gulch has an alluvial fan that is 1.8 km wide.
<b>Garlock fault along the Summit Range</b>							
D	11.24 ± 0.43 Ma ( <sup>40</sup> Ar/ <sup>39</sup> Ar biotite) orthoclase megacrystic dacite lava dome in Summit Range, overlying ca. 12 Ma basalt lava flows	0.00	MDS <sup>††</sup>	11.383 ± 0.028 Ma (U-Pb) orthoclase megacrystic dacite dike swarm in granitic rocks (Murdoch and Webb, 1940; Samsel, 1962)	43.7 [± 0.8]	11.383 [± 0.028]	These are much slower than neotectonic rates on the Garlock fault in this area (McGill et al., 2009)
C''	Easternmost exposures of clast assemblage in conglomerate of Hardcash Gulch. Also rounded textures and placer gold.	0.00	DSF <sup>††</sup>	Correlate to Dove Spring Formation in the western El Paso Mountains	40 [± 10]	7.5 to 11.8	This correlation has low precision because there are no specific features to restore
			C'	Deposition across Garlock fault from Goler Gulch which cuts clast sources of Goler Formation and Cudahy Camp Formation. See text discussion.	15.5 [± 0.9]	1.8 to 6.5	Similar source interpretation as the conglomerate of Golden Valley
<b>Savoy fault</b>							
D	11.24 ± 0.43 Ma ( <sup>40</sup> Ar/ <sup>39</sup> Ar biotite) orthoclase megacrystic dacite lava dome in Summit Range, overlying ca. 12 Ma basalt lava flows	2.30	D'	11.221 ± 0.18 Ma ( <sup>40</sup> Ar/ <sup>39</sup> Ar sanidine) orthoclase megacrystic dacite dome in Lava Mountains overlying ca. 12 Ma basalt lava flows	16.7 [± 1.8]	11.221 [± 0.018]	These domes are covered by younger dacite lavas and younger volcanic-sedimentary successions
E	~80-m-thick tuff bed in upper Bedrock Spring Formation	0.00	E'	~70-m-thick tuff bed within the Bedrock Spring Formation in Summit Range with ESE strike	6.0 [± 0.7]	7.479 to 0.9	Age from U-Pb zircon age of thick tuff in lava Mountains, sample JDW-20
F	Red plagioclase porphyritic lava flow with pliotaxitic fabric and basal vitrophyre deposited on top of 10–11 Ma dacite lavas	0.60	F'	Red plagioclase porphyritic lava flow with pliotaxitic fabric and basal vitrophyre over Bedrock Spring Formation	7.3 [± 1.3]	6.522 to 1.3	Age from U-Pb zircon age of vitrophyre in Lava Mountains, sample LV051810-8
					10.7 [± 2.5]	3.742 to 3.4	Subtracted tuff bed offset from megacrystic dacite dome offset for slip between 11.4 and 7.5 Ma

(continued)



TABLE 4. SLIP CONSTRAINTS FOR FAULTS IN LAVA MOUNTAINS–SUMMIT RANGE AREA (continued)

Label*	Slip constraint geologic feature		Correlated feature on opposite side of fault		D <sup>†</sup> (km)	Label*	Description	D <sup>†</sup> (km)	Slip (km) <sup>§</sup> [error]	Age (Ma) <sup>§</sup> [error]	Slip rate (mm/yr)	Notes
	Description	Description										
<b>Browns Ranch fault zone</b>												
G	Eastern edge of Lava Mountain Dacite lava flow overlying Bedrock Spring Formation	Eastern edge of Lava Mountain Dacite lava flow overlying Bedrock Spring Formation	G'	0.62	1.83	G'	3.9 [± 0.7]	6.522 [± 0.026]	0.5 to 0.7	Estimated slip restoring edge of 80–100-m-thick lava flow across wide fault zone		
<b>Blackwater fault</b>												
H	4-m-thick bluish pumice lapilli tuff of the distal facies of the Almond Mountain Volcanics. This bed dips moderately to the southeast.	4-m-thick bluish pumice lapilli tuff bed of the distal facies of the Almond Mountain Volcanics, dips 52° into fault zone	H'	0.00	1.13	H'	1.9 [± 0.3]	7.479 [± 0.023]	0.2 to 0.3	Tuff correlation to the thick tuff with a U-Pb zircon age. The fault zone is 480 m wide.		
I	ENE-striking buttress unconformity of Bedrock Spring Formation against side of dacite domes	ENE-striking buttress unconformity of Bedrock Spring Formation against the side of dacite domes	I''	0.1	0.1	I''	2.1 [± 0.6]	7.5 to 7.8		Note, there are three strands denoted by I', I'' and I'''		
J	North edge of thick glassy dacite lava flow over quartz monzonite	North edge of thick glassy dacite lava flow over quartz monzonite	J'	0.0	0.0	J'	0.3 to 1.8	7.2 [± 1.1]		From Oskin and Iriondo (2004)		
BM <sup>††</sup>	Northern edge of basalt lava flow	Northern edge of basalt lava flow	BM <sup>††</sup>	0.0	0.1	BM <sup>††</sup>	1.8 [± 0.1]	3.77 [± 0.11]		From Oskin and Iriondo (2004)		
<b>Garlock fault between El Paso Mountains and Pilot Knob area</b>												
MC <sup>††</sup>	Metaconglomerate of the Robbers Mountain Formation on east side of a fault with Devonian(?) greenstone (Carr et al., 1997)	Metaconglomerate of the Robbers Mountain Formation on the east side of a fault contact with greenstone (Carr and Poole, 1992)	PKV <sup>††</sup>	1.57	0.68	PKV <sup>††</sup>	62.7 [± 1.7]	ca. 260		Total slip across the central Garlock fault zone: includes El Paso fault and all of the faults in the Lava Mountains–Summit Range (LMSR)		
ECDS <sup>††</sup>	18 Ma "high-silica rhyolite dikes" in the Eagle Crags (Sabin, 1994; Monastero et al., 1997). Azimuth of 281, and 990 m wide.	Early Miocene(?) felsic dike swarm in the Sierra Nevada (Samsel, 1962). Azimuth of 289, and 980 m wide.	SESD <sup>††</sup>	18.5	0.37	SESD <sup>††</sup>	67.6 [+5.1/–3.8]	ca. 18		Total slip of the central Garlock fault zone: includes El Paso fault, faults in the LMSR, and Cliff Canyon fault		
<b>Inferred fault south of Christmas Canyon</b>												
							29.8 [± 1.1]	6.5 to 11.4	5.9 to 6.2	Subtracted offset of Christmas Canyon Paleozoic rocks to El Paso Mountains from the offset of the El Paso Mountains to Pilot Knob		

\*Label identifies slip constraint features shown on Figure 11.

<sup>†</sup>D is the projection distance of the feature to the fault.

<sup>§</sup>The amount of fault slip was measured using map data in a georeferenced ArcGIS database projected in Universal Transverse Mercator Zone 11 North. The fault slip constraints were projected to the fault trace, and the distance between them was measured along the trace of the fault. The slip amount shown is our preferred offset measurement. The error measurement is the interpreted maximum and minimum extreme geometric extrapolations of slip markers to the fault trace in question, and it encapsulates errors in exact correlation of specific points of line and area features, errors in horizontal projection using feature azimuths, and uncertainties associated with elevation differences.

<sup>††</sup>This is the age of the fault-slip constraint geologic feature.

\*\*We use the "meta- + (sedimentary rock)" terminology of Carr et al. (1997), because this best describes these rocks that retain sedimentary textures but have been partially recrystallized.

<sup>†††</sup>These constraints are located outside the area of Figure 11; see Figure 1 for their locations.

the north side of the fault. There is, however, a 1.3-km-wide swarm of north-trending dacitic dikes in the southeastern Sierra Nevada (Samsel, 1962; MDS on Fig. 1) that has a similar phenocryst assemblage and orthoclase megacrysts (Murdoch and Webb, 1940). These dikes could be feeder dikes for the megacrystic dacite dome in the Summit Range. A sample from these dikes has a U-Pb zircon age of  $11.383 \pm 0.028$  Ma (Fig. 5F; Table 3), compared to the  $11.24 \pm 0.43$  Ma  $^{40}\text{Ar}/^{39}\text{Ar}$  age of the megacrystic dacite lava in the Summit Range (Fig. 4H). These domes and dikes are the same age within error. The slip of the Garlock fault required to juxtapose the orthoclase megacrystic dikes of the Sierra Nevada to orthoclase megacrystic dacite domes in the Summit Range is  $43.7 \pm 0.8$  km (Table 4).

The Bedrock Spring Formation of the LMSR has been correlated with the upper Dove Spring Formation in the El Paso Mountains (DSF on Fig. 1) (Smith et al., 2002; Frankel et al., 2008). We find that the Bedrock Spring Formation matches well in time, composition, and sediment transport direction (Smith, 1964; Loomis and Burbank, 1988; Whistler et al., 2009) with member 5 of the Dove Spring Formation. The lower four members of the Dove Spring Formation correlate in time with the Summit Range volcanics, but these do not have dacite lava domes or the associated near-vent volcanic rocks. An  $11.8 \pm 0.9$  Ma (Loomis and Burbank, 1988) thick felsic tuff occurs in member 2 of the Dove Spring Formation, which could have erupted from the lava domes of the Summit Range volcanics (Frankel et al., 2008). These correlations loosely constrain offset of the Garlock fault to be 30–50 km (Table 4).

The Pliocene conglomerate of the Hardcash Gulch contains clasts consistent with a source from Goler Gulch in the eastern El Paso Mountains (Fig. 11) based on the presence of exotic clasts, well-rounded textures of boulders, and placer gold (see earlier discussion of Pliocene conglomerates). Garlock fault offset needed to deposit the easternmost exposure of the conglomerate of Hardcash Gulch is  $15.5 \pm 0.9$  km (C'' to C' on Fig. 11; Table 4). The age of this conglomerate is unknown, but it is younger than the Lava Mountain Dacite–correlated intrusive rocks it overlies, and the western parts may be as young as early Pleistocene. Slip-rate calculations for minimum and maximum values yields 2.2–9.1 mm/yr (Table 4). The younger ages therefore are more consistent with the neotectonic slip rates for the central Garlock (McGill and Sieh, 1993; Rittase et al., 2014).

**Teagle Wash fault.** There are no fault slip markers for the Teagle Wash fault. The presence of Jurassic Laurel Mountain granodiorite below

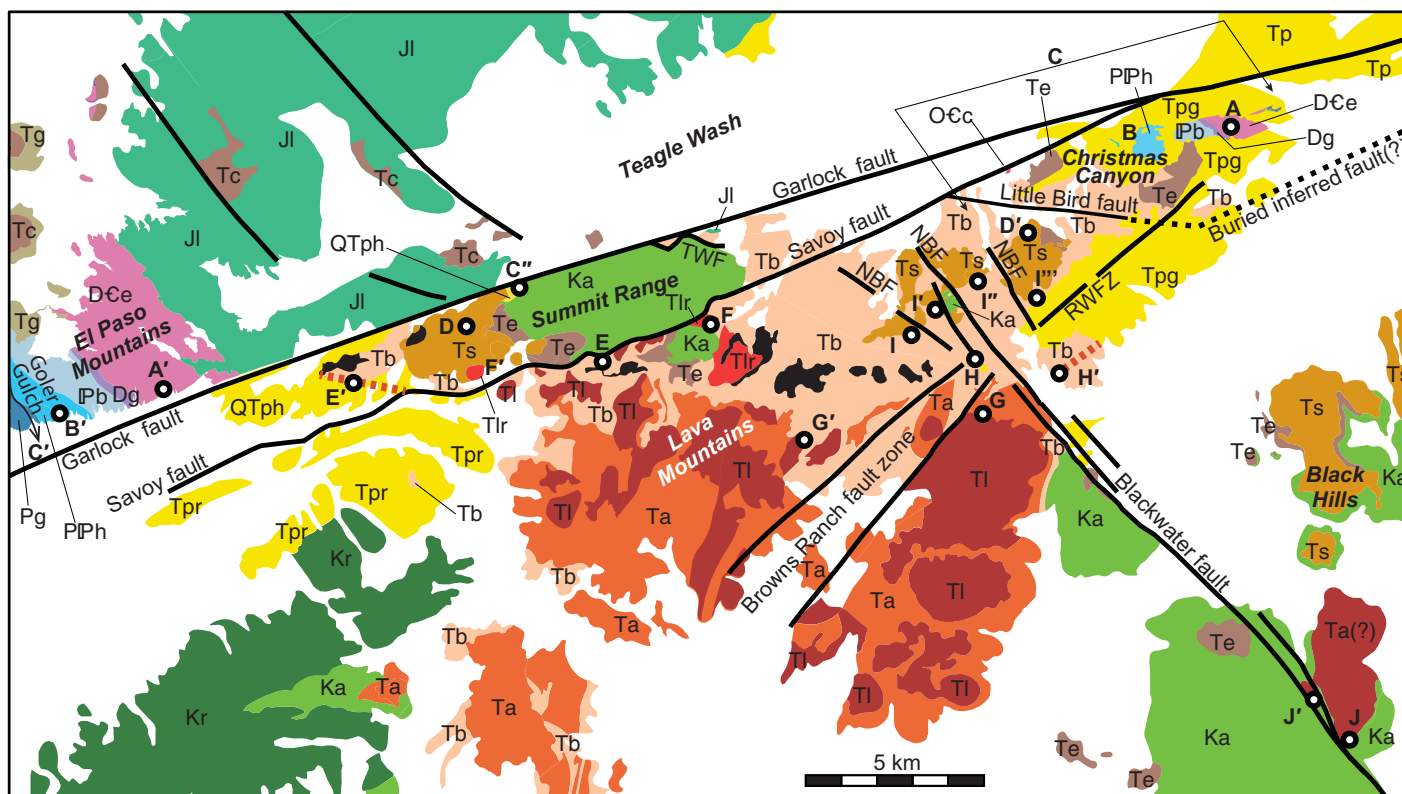


Figure 11. Fault-slip restoration points plotted on the simplified geologic map of the Lava Mountains–Summit Range (Fig. 2). The labeled thick circles are reconstruction points for slip constraints derived from this new study, where, for example, X restores adjacent to X', X'', and X''' (see text and Table 4 for descriptions). Slip marker C is the outcrop area of the conglomerate of Golden Valley along the Garlock fault.

this fault requires a much larger amount of strike slip, because the map distance, as measured on the north side of the Garlock fault, between the Jurassic granodiorite in the eastern El Paso Mountains and the Atolia Quartz Monzonite–correlated plutons in the Sierra Nevada is 34 km (Fig. 1).

**Savoy fault.** The Savoy fault cuts all of the Miocene and Pliocene units of the LMSR. The only locations of Summit Range volcanics with ca. 12 Ma basalt flows overlain by ca. 11 Ma dacite dome complexes are in the central Summit Range and in the northeastern Lava Mountains. Dacite lava with distinctive megacrystic orthoclase occurs in the central Summit Range (D on Fig. 11) with an age of  $11.24 \pm 0.43$  Ma (Fig. 4H) and also in the northeastern Lava Mountains (D' on Fig. 11) with an age of  $11.221 \pm 0.018$  Ma (Fig. 4I). We correlate these dacites along with their associated lava domes and basalt flows of Summit Range volcanics across the Savoy fault for left-lateral offset of  $16.7 \pm 1.8$  km (Table 4). The megacrystic dacite in the Summit Range correlates to the megacrystic dacitic dikes in the Sierra Nevada that have a U–Pb zircon age of  $11.383 \pm 0.028$  Ma; therefore we take ca. 11.4 Ma as the best age for

the megacrystic dacite in the Lava Mountains and for the age constraint of the offset on the Savoy fault.

Younger units can be correlated across the Savoy fault. An 80-m-thick tuff bed occurs in the upper part of the Bedrock Spring Formation in the Lava Mountains where it is cut by the Savoy fault (E on Fig. 11). A similarly thick tuff bed within Bedrock Spring Formation is exposed in the western Summit Range (E' on Fig. 11). The offset needed to juxtapose these tuff beds is  $\sim 6.0 \pm 0.7$  km (Table 4). The age of this tuff bed is unknown, but we interpret it to correlate to the only other thick tuff within the Bedrock Spring Formations, which has an age of  $7.479 \pm 0.023$  Ma (Fig. 5C). The distinctive red flow-banded lava flow of the 6.5 Ma Lava Mountain Dacite can also be correlated across the Savoy fault (F and F' on Fig. 11, respectively), requiring  $7.3 \pm 1.3$  km of slip (Table 4), similar within error to that of the tuff offset. Because we have offset markers of different ages, we can calculate two intervals of slip (Table 4). Combining these yields slip in the interval between 11.2 and ca. 7 Ma of  $10.7 \pm 2.5$  km. Using the total slip estimate above for the fault yields motion of  $\sim 6$  km between ca. 7 Ma and present.

**Brown's Ranch fault zone.** Determining slip for the Brown's Ranch fault zone is difficult because it is oriented parallel to the strike of the upper Miocene units. There is an apparent offset of the Lava Mountain Dacite in map view (Figs. 2 and 11; Table 4). We estimate that  $3.9 \pm 0.7$  km of left-lateral offset is needed to restore the eastern edge of the exposures of the Lava Mountain Dacite (G and G' on Fig. 11; Table 4) across the Brown's Ranch fault zone.

**Little Bird fault.** The Little Bird fault does not have any specific geologic features that can be used to measure offset across it. It juxtaposes Paleozoic metasedimentary rocks with Cretaceous granitic rocks; these rocks are  $>26$  km apart to the north of the Garlock fault.

#### Dextral Fault

**Blackwater fault.** The facies of the Almond Mountain Volcanics are mismatched across the northern portion of the Blackwater fault. East of the Blackwater fault there is only a single bluish-colored pumice lapilli tuff bed within the Bedrock Spring Formation (H on Fig. 11). This tuff dips southwest at a moderate angle, is  $\sim 4$  m thick, and is part of the distal facies of the Almond Mountain Volcanics. The west side of

the Blackwater fault exposes both the distal and near-vent facies of the Almond Mountain Volcanics. At the northern extent of volcanic debris-flow units in the Bedrock Spring Formation there is a 4–5-m-thick tuff that ends eastward at the Blackwater fault (H' on Fig. 11). This same tuff bed is dextrally offset in repeated slivers across a ~600-m-wide fault zone. Total offset of the tuff is  $1.9 \pm 0.3$  km (Table 4).

Farther north along the projection of the Blackwater fault there are right-lateral offsets of the northeast-striking buttress unconformity of the Bedrock Spring Formation deposited against the steep southern sides of the lava domes of the Summit Range volcanics (I, I', I'' and I''' on Fig. 11). The total offset of these points across the zone of faulting is  $2.1 \pm 0.6$  km (Table 4). The lava domes partially blocked the northward flow in the basin of the Bedrock Spring Formation as shown by the presence of lacustrine limestone only along this northeast-trending buttress unconformity. These ~2 km right-lateral slip values are similar to those obtained by Oskin and Iriondo (2004) from farther south along the Blackwater fault (Table 4) using slip markers of  $7.2 \pm 1.1$  Ma (J to J', Fig. 11) and  $3.77 \pm 0.11$  Ma (BM on Fig. 1).

### Regional Garlock Fault

Additional slip markers are needed for the central Garlock faults to evaluate the fault slip in the LMSR. The Paleozoic rocks in the El Paso Mountains have been correlated to similar Paleozoic rocks in the Pilot Knob area (Fig. 1) for a left-lateral offset of 48–64 km on the central Garlock fault (Smith and Ketner, 1970; Carr et al., 1997; Table 1). Geologic map data show a steeply dipping fault in the El Paso Mountains that places Mississippian meta-conglomerate of the Robbers Mountain Formation against Devonian(?) greenstone (Carr et al., 1997). A steeply dipping fault in the Pilot Knob area juxtaposes the same units (Carr and Poole, 1992). Matching these faults (MC and PKV, respectively, on Fig. 1) yields  $62.7 \pm 1.7$  km of offset (Table 4).

Another offset marker for the central Garlock fault is an 18 Ma swarm of WNW-striking, “high-silica rhyolite dikes” (ECDS on Fig. 1) in the Eagle Crags (Sabin, 1994; Monastero et al., 1997). A set of dikes with similar width, azimuth, and composition occurs in the southeastern Sierra Nevada (SESD on Fig. 1) intruded into Cretaceous granite (Samsel, 1962). These dikes are correlated to early Miocene volcanism (Dibblee, 1967), as this swarm projects into a lower Miocene volcanic center (Coles et al., 1997). A slip marker using these dikes yields  $67.6^{+5.1/-3.8}$  km left-lateral slip on the central Garlock fault (Table 4).

## IMPLICATIONS FOR THE CENTRAL GARLOCK FAULT ZONE

### Inferred Fault South of Christmas Canyon

The slip data for Paleozoic rocks at Christmas Canyon require the presence of an unexposed fault south of the Christmas Canyon area. These Paleozoic rocks do not continue southward, as the Black Hills have Cretaceous Atolia Quartz Monzonite as basement (Fig. 11). A large exposure of Paleozoic rocks occurs east of the LMSR on the south side of the Garlock fault in the Pilot Knob Valley area (PKV on Fig. 1), which are offset  $62.7 \pm 1.7$  km (Table 4) from the El Paso Mountains. There are no direct ties of the Paleozoic rocks of Christmas Canyon with the Pilot Knob area, but the Christmas Canyon rocks are displaced  $32.9 \pm 0.6$  km from the El Paso Mountains by the Garlock fault. Thus, a fault with 29.8 km of left-lateral slip (Table 4) presumably exists south of Christmas Canyon to restore it to Pilot Knob Valley.

Based on outcrop patterns, this inferred fault must have a ENE strike in an area that is covered by the Pliocene conglomerate of Golden Valley and Quaternary alluvial deposits. This conglomerate overlaps the Little Bird fault and probably also the inferred fault. Juxtaposition of the Christmas Canyon area to the north of the Black Hills by this inferred fault was completed prior to deposition of the capping basalt boulder layer of the conglomerate of Golden Valley because it has basalt clasts without dacite lava clasts; the Black Hills are the only exposure of ca. 12 Ma basalt without overlapping dacite domes (Fig. 2).

### Initiation of the Garlock Fault Zone

Slip markers in the LMSR yield offsets for the Garlock fault that differ from the total offset of ~64 km (Table 1). Sinistral slip on the Garlock fault required to juxtapose the megacrystic dacite domes in the Summit Range with megacrystic dikes in the Sierra Nevada is  $43.7 \pm 0.8$  km (Table 4), whereas ca. 18 Ma high-silica dikes southeast of the LMSR appear to record the full offset of the Garlock ( $67.6^{+5.1/-3.8}$  km) to the Sierra Nevada. This difference may be explained in two ways: (1) the Garlock fault slip began between 18 and 11.4 Ma, so the megacrystic dacite is too young to record the full Garlock fault offset; or (2) slip in the vicinity of the LMSR is distributed among several faults, with the megacrystic dacites of the Summit Range within and the 18 Ma dikes outside of this fault zone. We favor the second hypothesis because of the presence of several faults with left-lateral offset within the LMSR: the Savoy fault has

$16.7 \pm 1.8$  km of slip of ca. 11.4 Ma features (see the age discussion in the “Magnitude and Rates of Fault Slip” section), and the Brown’s Ranch fault zone has  $3.9 \pm 0.7$  km of slip of ca. 6.5 Ma features (Table 4). Adding these offsets to the 43.7 km offset for the Summit Range segment of the Garlock fault gives cumulative left-lateral slip of 64.3 km, similar to the ~64 km total slip value derived from Paleozoic, Mesozoic, and early Miocene offset markers outside the distributed zone of faulting of the LMSR (Table 1). This amount of slip supports the interpretation that motion on the Garlock fault began at or after ca. 11 Ma (e.g., Burbank and Whistler, 1987) and that sinistral slip is distributed across a 12-km-wide fault zone. Thus, for this area we refer to the sinistral faults together as the Garlock fault zone (GFZ).

### Initiation of Regional Dextral Shear

The GFZ is embedded in an active zone of dextral shear (see references in Gan et al., 2003). Initiation of dextral shear occurred in Death Valley, to the east of the LMSR (Fig. 1), at ca. 7 Ma (Holm et al., 1993; Topping, 1993), although Mancktelow and Pavlis (1994) argued that this initiated at ca. 11 Ma. The initiation age is younger in areas west of Death Valley: ca. 4 Ma in Panamint and Searles Valleys (Burchfiel et al., 1987; Hodges et al., 1990; Zhang et al., 1990; Snyder and Hodges, 2000; Walker et al., 2014), and 2–3 Ma farther to the west in Indian Wells Valley (Monastero et al., 2002). This westward migration of dextral shear possibly also occurred in the Eastern California shear zone, but the initiation ages are poorly known: beginning after 6 Ma (Dokka and Travis, 1990; Schermer et al., 1996; Glazner et al., 2002), 3.8 Ma (Oskin and Iriondo, 2004), or even younger (Miller and Yount, 2002). The age of the initiation of dextral shear in the LMSR is interpreted to be <3.8 Ma, the time for initiation of the dextral slip on the Blackwater fault (Oskin and Iriondo, 2004; this paper), similar to ca. 4 Ma initiation in Searles Valley (Fig. 1) just north of the LMSR.

### Change in Deposition Systems

There is a profound change in the deposition systems along the GFZ after ca. 7 Ma. The Bedrock Spring and Dove Spring Formations along the central GFZ are thick successions of arkosic sandstone deposited from 11.5 to 7.0 Ma (Fig. 12), with sediment transported northwestward from granitic bedrock sources in the central Mojave Desert area (Smith, 1964; Loomis and Burbank, 1988; Whistler et al., 2009; this paper). The conglomerate of Golden Valley occurs as a



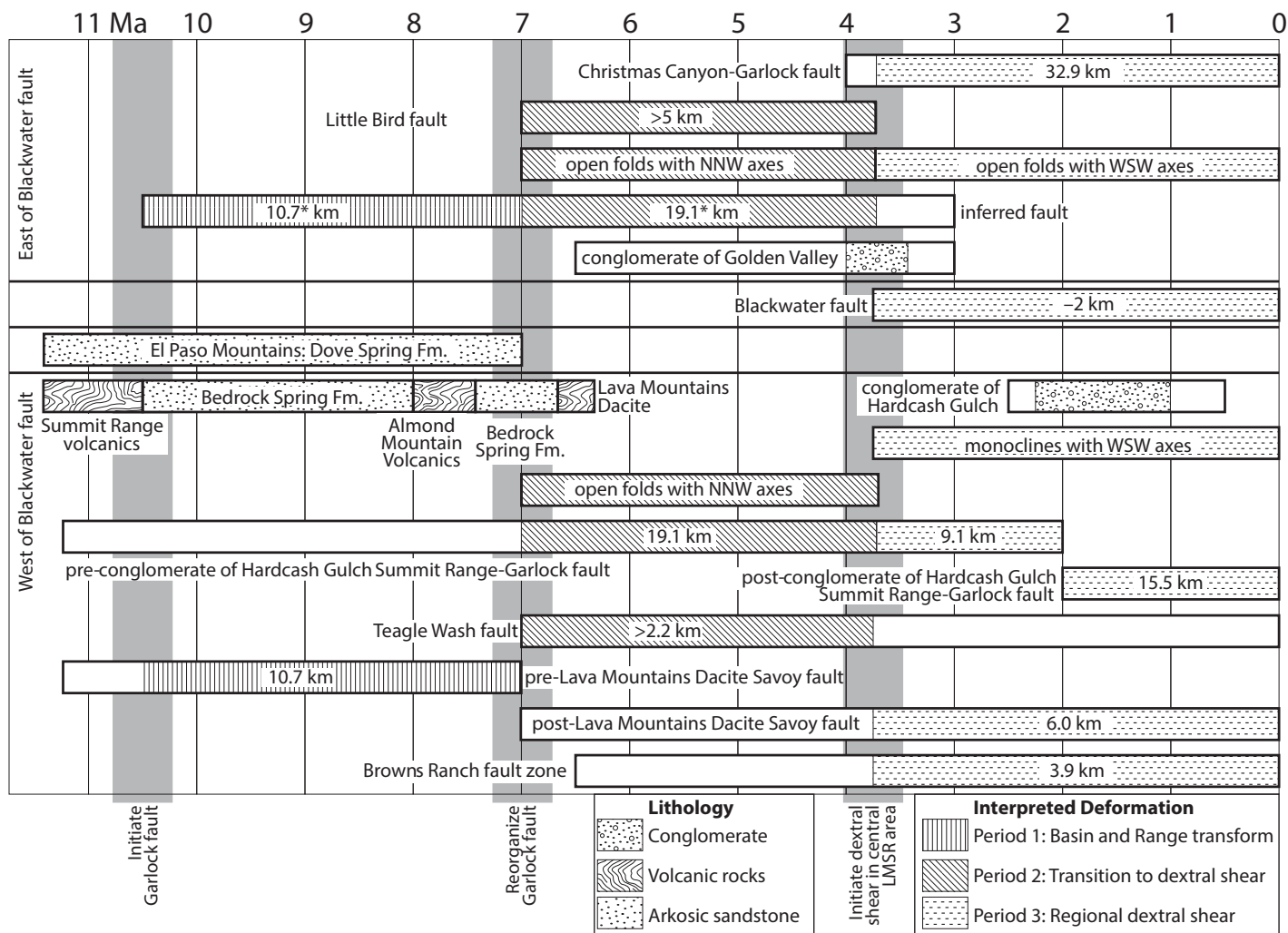


**Figure 12.** Summary of timing constraints for the Lava Mountains–Summit Range (LMSR) area. Faults, rock units, and folds are arranged from east to west relative to the Blackwater fault. Box outlines denote the maximum and minimum timing constraints for rock units and deformation. Pattern fills indicate the interpreted timing of each feature based on the three-stage deformation history model of the Garlock fault zone. The slip amount interpreted for each fault in each stage is given. Slip amounts are negative for dextral slip, and amounts with asterisks are calculated from other slip constraints. The vertical gray bars denote key times in the history. The 9.1 km for the Garlock fault between 4 and 2 Ma is derived by subtracting the total slip of the Summit Range segment of the Garlock fault and subtracting the 7–3.8 Ma and 2–0 Ma slip values (19.1 km and 15.5 km, respectively) for the same fault.

local basin sourced from a now-displaced local uplift along the GFZ, as discussed above. The modern deposition systems along the GFZ are similar, having local closed basins and sediment sources in nearby uplifts (Fig. 1). The topography of the central GFZ therefore changed from one of low relief that did not significantly disturb transport and deposition to a system with locally high relief creating uplifts and closed basins. We postulate that the change to dextral shear could have led to creation of higher-relief topography along the GFZ, and therefore this conglomerate may have formed during the initiation of local dextral shear at ca. 3.8 Ma (Oskin and Iriondo, 2004).

### Current Structural Configuration of the Garlock Fault Zone

The configuration of faults is different on either side of the Blackwater fault (Fig. 11): to the west, the Summit Range segment of the Garlock fault is active, with additional slip on several other sinistral strike-slip faults (Teagle Wash fault, Savoy fault, and Brown's Ranch fault zone); to the east, there are only the Garlock and dip-slip Randsburg Wash faults. The Garlock, Savoy, and Randsburg Wash faults are all correlated with Quaternary fault scarps, and the Brown's Ranch fault zone was interpreted by Smith (1964) to have young slip. The

Teagle Wash fault is somewhat different and has more similarity with the Little Bird fault in that it juxtaposes different-age basement rocks (i.e., Cretaceous versus Jurassic), implying a significant left-lateral slip. Slip on the Teagle Wash fault resolves onto the Savoy and Garlock faults, and so its history is not critical to this analysis. WSW-trending folds occur in all Miocene (Figs. 9J and 9K) and Pliocene (Fig. 9L) rock units and have been interpreted to have been active as recently as the Pleistocene (Smith, 1964, 1991).

This young deformation can be more fully explored in the context of a regional deformation model. The model is based on two obser-

vations: (1) the trace of the Garlock is curved; and (2) dextral faults in the areas to the north and south do not cut the Garlock (i.e., slip on the Blackwater fault ends northward before the Garlock fault). The curved trace of the Garlock fault is an outcome of progressive bending of an originally northeast-trending fault by transversely oriented dextral shear distributed along the central and eastern segments (Garfunkel, 1974; Dokka and Travis, 1990; Gan et al., 2003). Young deformation in the LMSR must accommodate the dextral faulting of the Blackwater fault without cutting the Garlock fault as well as larger-scale clockwise bending of the trace of the Garlock fault.

Accommodation of dextral slip in the LMSR necessitates NNW-SSE-oriented shortening of western side of the Blackwater fault relative to the eastern side. The NNW-SSE shortening could be taken up by the WSW-trending folding and also by lateral escape of fault slivers between the Summit Range segment of the Garlock fault, the Savoy fault, and the Brown's Ranch fault zone (Fig. 11). NNW-SSE elongation east of the Blackwater could be partially taken up by normal slip on the Randsburg Wash fault. These deformation mechanisms would absorb the slip of the Blackwater so that the Garlock fault is not offset and would allow the trace of the Garlock to be bent by increasing clockwise amounts eastward.

The slip history of faults in the Christmas Canyon appears to also fit with this dextral slip accommodation model. The Paleozoic rocks of the Christmas Canyon area were north of the main trace of the GFZ system until after deposition of the conglomerate of Golden Valley when the Christmas Canyon segment of the Garlock fault formed. Block transfer across the GFZ by a left step in the main trace of the GFZ effectively adds material to the east side of the Blackwater fault. This breaking of a new fault also allows a more continuous trace to the active strand of the Garlock fault. We envision that these processes could apply to other intersections of dextral faults with the GFZ and possibly to the larger-scale clockwise bending of the trace of the Garlock fault. This model implies that the wide, multiple-fault structure of the GFZ formed in response to dextral slip of the Blackwater fault, which began after 3.8 Ma (Oskin and Iriondo, 2004; this paper).

### Slip History of the Garlock Fault Zone

The current structural configuration of the LMSR, as outlined above, implies a link between the wide, multi-stranded GFZ and the accommodation of dextral slip and clockwise bending of the Garlock. Therefore defor-

mation older than 3.8 Ma in the LMSR does not accommodate dextral slip. Unfortunately, long-lived strike-slip fault systems like the GFZ do not preserve a complete detailed history of slip. To aid interpretation we assume that the older GFZ was a simple strike-slip fault with only one active fault strand because it did not need to accommodate dextral slip and shear (see Fig. 12 for interpreted timing of fault slip and Fig. 13 for interpreted time-slice maps). The single-strand assumption is supported by observing that the western Garlock fault has this character and is outside the zone of dextral shear.

The slip constraints from the LMSR using the volcanic-sedimentary assemblages as the key time markers allow a view of two increments in the pre-3.8 Ma history of the GFZ. The oldest offset markers are ca. 11.4 Ma megacrystic dacite domes and feeder dikes, but the relative locations of slightly younger (10.5 Ma) dacite domes across the Savoy fault could give a better maximum age. The end of deposition of the Bedrock Spring Formation demarks the end of the early slip of the Savoy fault and the beginning of slip on the Little Bird fault. The 7.5 and 6.5 Ma slip markers for the Savoy fault have indistinguishable offsets within error; for simplicity in this discussion, we average these ages to ca. 7 Ma. The next-younger marker unit is the conglomerate of Golden Valley whose age is not well known. We interpret its deposition to be linked with the beginning of the dextral deformation, because the same deposition system that created this conglomerate is still active from Goler Gulch. We assume that deposition began at ca. 4 Ma in this analysis.

These assumptions allow a glimpse of the earlier slip history of the GFZ. The earliest slip was 10.7 km on the Savoy from 10.5 to ca. 7 Ma. This amount of slip was taken up in the eastern LMSR on the inferred fault discussed above. Afterward from ca. 7 Ma until 3.8 Ma, slip occurred on the Summit Range segment of the Garlock, Teagle Wash, and Little Bird faults and the inferred fault. The intermediate-stage GFZ had a maximum sinistral slip of 19.1 km (subtraction of the 10.7 km of Savoy fault slip from the 29.8 km calculated slip for the inferred fault) if the Summit Range segment of the Garlock fault was active only after the first stage of slip on the Savoy fault. NNW-trending folds formed during the intermediate-stage slip in the areas along the Little Bird fault. We speculate that this fold set may be due to the ESE strike of the Little Bird fault. This orientation would have caused the Little Bird fault to have a restraining orientation in the sinistral fault system, forming NNW-trending folds.

### Garlock Fault Zone Slip Rates

Slip rates calculated in Table 4 are based on the minimum and maximum timing constraints for fault motion, but these do not specify when the faults were active. When these slip estimates are considered in light of the three-stage deformation scenario proposed above (Fig. 12), we can use the entire data set to estimate slip rates within the fault system. The earliest stage involved the Savoy fault with a slip rate of 3.1 mm/yr (10.7 km over the interval from 10.5 to ca. 7 Ma). If the single-strand assumption for the early Garlock fault is not true, then additional slip would have occurred on the Summit Range segment of the Garlock fault at this time, which would increase the slip rate for this interval. The slip rate for the Garlock fault in the intermediate stage is a maximum of 6.0 mm/yr (19.1 km over the interval from ca. 7 to 3.8 Ma); this rate would decrease if some slip on these faults occurred in the earlier stage. Youngest-stage slip in the eastern LMSR is interpreted to have been on the Christmas Canyon segment of the Garlock fault with a slip rate of 8.7 mm/yr (32.9 km since 3.8 Ma). This slip-rate acceleration is linked to the initiation of dextral faulting in the LMSR area. West of the Blackwater fault the sinistral slip of the GFZ is divided across three main faults and fault zone: the Summit Range segment of the Garlock fault (43.7 km – 19.1 km = 24.6 km of slip) has a rate of 6.5 mm/yr, the Savoy fault (6.0 km of slip) has a rate of 1.6 mm/yr, and the Brown's Ranch fault zone (3.9 km of slip) has a rate of 1.0 mm/yr.

The distribution of sinistral slip across multiple faults in the western LMSR creates discrepancies in the slip rates along the modern GFZ. The single-stranded Garlock fault east of the LMSR has neotectonic slip rates, depending on the age of the marker, of 4–9 mm/yr (McGill and Sieh, 1993) and 7–14 mm/yr (Rittase et al., 2014), which match with our longer-term, model-interpreted slip rate of 8.7 mm/yr. West of the LMSR the neotectonic slip rates on the central Garlock fault are 4.5–6.1 mm/yr (Clark and Lajoie, 1974), which agrees with the model-calculated slip rate of 6.0 mm/yr for the Summit Range segment of the Garlock fault. Our model-calculated rates for the Summit Range segment of the Garlock fault plus those for the Savoy fault add to 7.6 mm/yr, which agrees with the 5.3–10.7 mm/yr neotectonic rate for the western segment of the Garlock fault (McGill et al., 2009).

### CONCLUSIONS

The LMSR area is a Miocene to Pliocene volcanic-sedimentary complex adjacent to the Garlock fault that contains rocks created before,

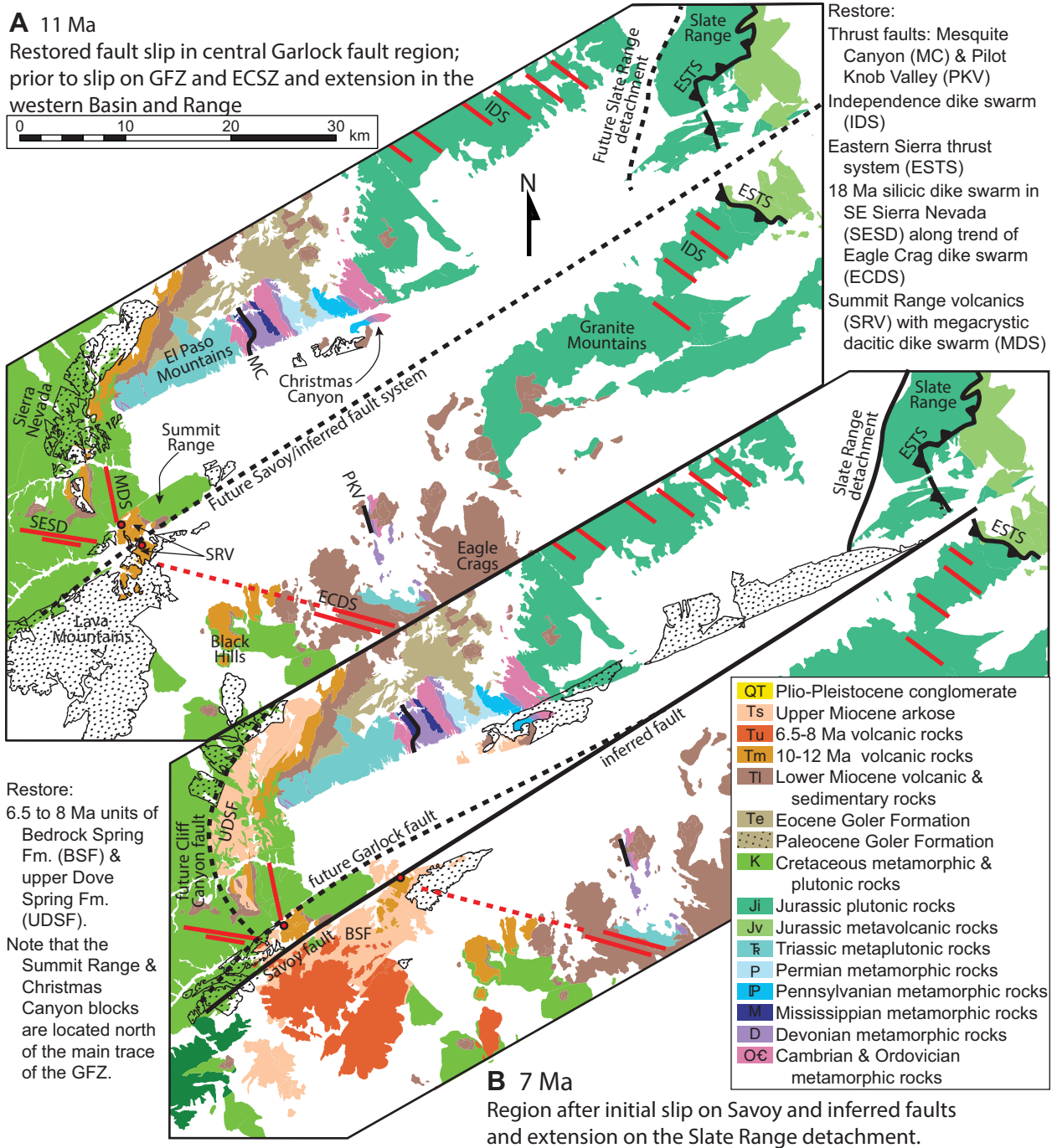


Figure 13 (on this and following page). Interpreted time-slice maps using new fault displacement data (Table 4) and interpreted fault slip chronology (Fig. 12). Thick black lines shown in each time slice are faults that were active before the time-slice figure, and dashed faults are active after. Red-filled dots are the locations of the megacrystic dacite lava domes in the Summit Range and Lava Mountains for each time-slice map. Note that rock unit labels are only on the time slice in D. The interval 4–0 Ma is interpreted to have local clockwise vertical-axis rotations; blocks with rotations are shown with a curved arrow in C. Panel D shows the area interpreted to be the wide active Garlock fault zone as diagonal hatching. Fault displacement data from the Slate Range are from Andrew and Walker (2009) and Andrew et al. (2011). Data for the Cerro Coso fault are from Casey et al. (2008) and Andrew et al. (2011). Data for the Cliff Canyon fault are reconnaissance data (collected by the authors of this study). The right-lateral slip of the Goldstone Lake fault is an interpreted amount in order to juxtapose and align the Eastern Sierra thrust system (ESTS) across the Garlock fault. GFZ—Garlock fault zone; ECSZ—Eastern California shear zone.



**C 4 Ma**

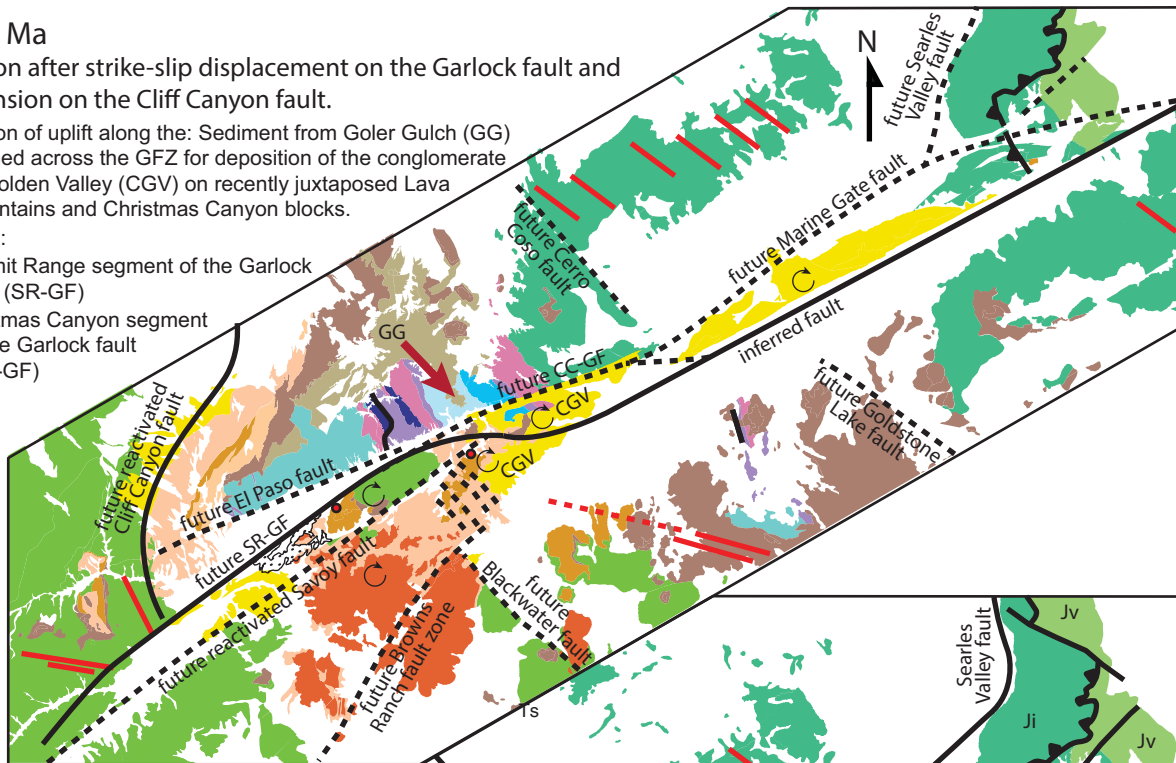
Region after strike-slip displacement on the Garlock fault and extension on the Cliff Canyon fault.

Initiation of uplift along the: Sediment from Goler Gulch (GG) is shed across the GFZ for deposition of the conglomerate of Golden Valley (CGV) on recently juxtaposed Lava Mountains and Christmas Canyon blocks.

Future:

Summit Range segment of the Garlock fault (SR-GF)

Christmas Canyon segment of the Garlock fault (CC-GF)



**D 0 Ma**

Region after initiation of ECSZ and the creation of the wide and complex Garlock fault zone.

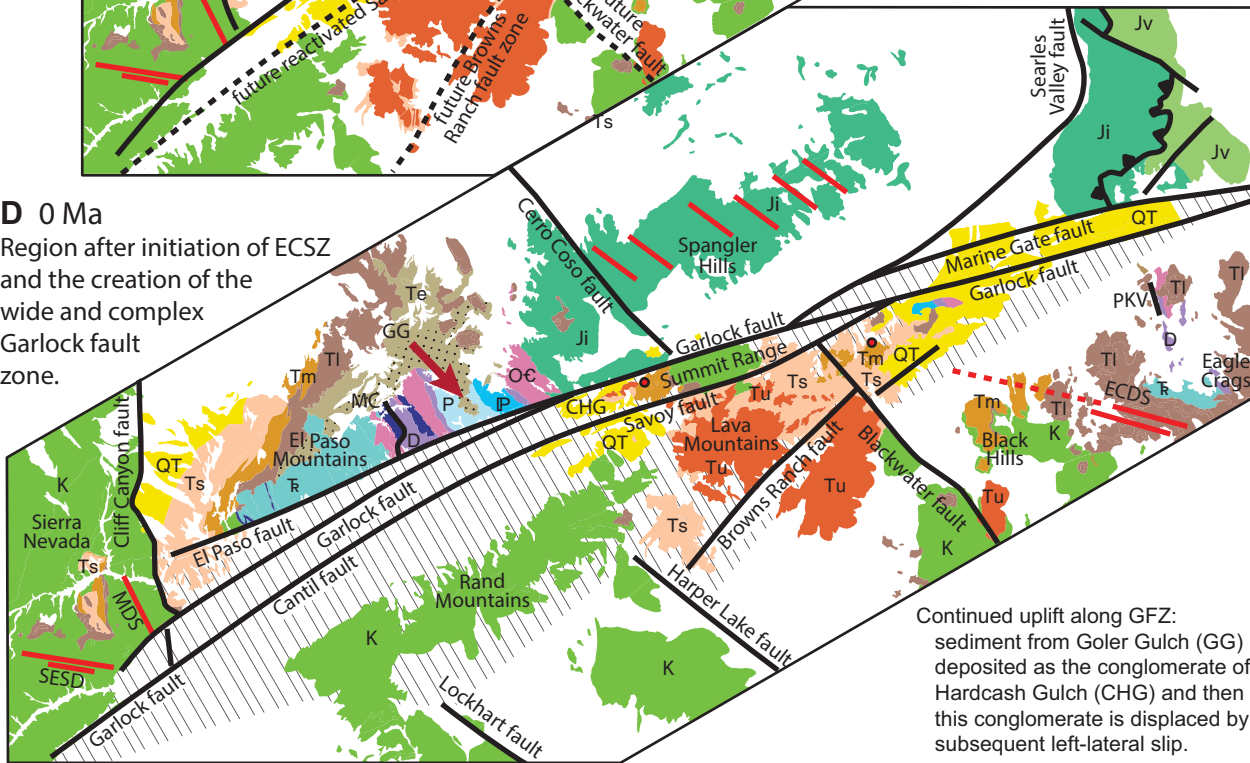


Figure 13 (continued).

during, and after slip on faults in the GFZ. Geologic features yield constraints on fault slip that indicate a three-stage history. The GFZ began as a single-stranded fault after 10.5 Ma with slip on the Savoy fault continuing eastward on a now-buried inferred fault south of Christmas Canyon. We interpret an intermediate stage of deformation between ca. 7 Ma and 3.8 Ma when the active strand of the GFZ became the Summit Range segment of the Garlock fault which con-

nected to the inferred fault via the Teagle Wash and Little Bird faults. The ESE strike of the Little Bird fault was a constrictional bend in the GFZ as recorded by NNW-trending folds. This constrictional bend was eventually abandoned as the sinistral fault system stepped leftward, creating the Christmas Canyon segment of the Garlock fault to the north of Christmas Canyon. The first and intermediate stages have ~30 km of cumulative sinistral slip. The last stage in the

slip history occurred after 3.8 Ma when the GFZ changed into a locally wide, multi-stranded fault zone to accommodate dextral offset of the Blackwater fault and regional clockwise oroclinal bending of the GFZ. This stage had ~33 km of slip on the GFZ, which is roughly half of the total offset. Topography along the GFZ changed at the beginning of this stage of deformation to one of local high relief, creating a new pattern of depositional systems. The slip rates for the

recent motion on the Garlock fault calculated using the three-stage deformation scenario are 6.0 mm/yr for the Summit Range segment and 8.7 mm/yr for the Christmas Canyon segment. The multi-stranded configuration of the GFZ west of the Blackwater fault explains the slower slip rate of the central Garlock fault along the El Paso Mountains (Clark and Lajoie, 1974) compared to sites east of the Blackwater fault (McGill and Sieh, 1993; Rittase et al., 2014) and farther west where the multi-stranded GFZ narrows to the single-stranded western Garlock fault.

The younger deformation system of the LMSR can be modeled as a zone of strain accommodation, taking up the 2 km of dextral slip on the Blackwater fault without cutting the Garlock fault. Although much of the regional dextral strain is accommodated by bending of the trace of the Garlock fault, the area of the LMSR must internally deform to allow bending of the Garlock fault trace and dextral offset of the Blackwater fault. The transfer of the Christmas Canyon block across the Garlock fault zone during the initiation of the last stage of slip may have been created by a deflection of the trace of the Garlock fault during the initial stages of regional dextral shear.

#### ACKNOWLEDGMENTS

This work was partly supported by a grant from the Geothermal Program Office of the U.S. Department of the Navy, China Lake, and the National Science Foundation EarthScope Program. Andrew Sabin and Steve Alm facilitated logistics and access permissions to areas of the China Lake Naval Weapons Station. Matt Heizler and the New Mexico Geochronology Research Laboratory provided analyses and interpretations for most of the argon data in this paper. Tands Bidgoli helped with early reviews of the paper. Finally, we acknowledge Jeff Lee, Terry Pavlis, and Nadine McQuarrie for comments leading to great improvement in the manuscript.

#### REFERENCES CITED

- Andrew, J.E., and Walker, J.D., 2009, Reconstructing late Cenozoic deformation in central Panamint Valley, California: Evolution of slip partitioning in the Walker Lane: *Geosphere*, v. 5, p. 172–198, doi:10.1130/GES00178.1.
- Andrew, J.E., Walker, J.D., and Monastero, F.C., 2011, Slip history model of the Garlock fault zone: Basin and Range extension overprinted by Eastern California shear zone transension: *Geological Society of America Abstracts with Programs*, v. 43, no. 2, p. 209.
- Andrew, J.E., Rittase, W.M., Monastero, F.M., Bidgoli, T., and Walker, J.D., 2014, Geologic map of the Northern Lava Mountains and Summit Range, San Bernardino County, California: *Geological Society of America Digital Map and Chart 19*, scale 1:20,000, doi:10.1130/2014.DMCH019.
- Blythe, A.E., and Longinotti, N., 2013, Exhumation of the southern Sierra Nevada—eastern Tehachapi Mountains constrained by low-temperature thermochronology: Implications for the initiation of the Garlock fault: *Lithosphere*, v. 5, p. 321–327, doi:10.1130/L252.1.
- Bowring, J.F., McLean, N.M., and Bowring, S.A., 2011, Engineering cyber infrastructure for U-Pb geochronology: Tripoli and U-Pb\_Redux: *Geochemistry, Geophysics, Geosystems*, v. 12, Q0AA19, doi:10.1029/2010GC003479.
- Brueseke, M.E., Heizler, M.T., Hart, W.K., and Mertzman, S.A., 2007, Distribution and geochronology of Oregon Plateau (USA) flood basalt volcanism: The Steens Basalt revisited: *Journal of Volcanology and Geothermal Research*, v. 161, p. 187–214, doi:10.1016/j.jvolgeores.2006.12.004.
- Burbank, D.W., and Whistler, D.P., 1987, Temporally constrained rotations derived from magnetostratigraphic data: Implications for the initiation of the Garlock fault: *Geology*, v. 15, p. 1172–1175, doi:10.1130/0091-7613(1987)15<1172:TCTTRDF>2.0.CO;2.
- Burchfiel, B.C., Hodges, K.V., and Royden, L.H., 1987, Geology of Panamint Valley—Saline Valley pull-apart system, California: Palinspastic evidence for low-angle geometry of a Neogene range-bounding fault: *Journal of Geophysical Research*, v. 92, p. 10,422–10,426, doi:10.1029/JB092iB10p10422.
- Carr, M.D., and Poole, F.G., 1992, Geologic map of the Tertiary rocks in Pilot Valley, California: U.S. Geological Survey Bulletin 2015, scale 1:24,000.
- Carr, M.D., Christiansen, R.L., Poole, F.G., and Gooch, J.W., 1997, Bedrock geologic map of the El Paso Mountains in the Garlock and El Paso Peaks 7.5' quadrangles, Kern County, California: U.S. Geological Survey Miscellaneous Investigations Map I-2389, scale 1:24,000 with pamphlet.
- Carter, B., 1994, Neogene offsets and displacement rates, central Garlock fault, California, in McGill, S.F., and Ross, T.M., eds., *Geological Investigations of an Active Margin: Redlands, California*, San Bernardino County Museum Association, p. 348–356.
- Casey, Z., Walker, J.D., and Taylor, M., 2008, Kinematics of the Cerro Coso fault and its intersection with the Garlock fault, southern Indian Wells Valley, CA: *Geological Society of America Abstracts with Programs*, v. 40, no. 1, p. 99.
- Chester, F.M., and Logan, J.M., 1987, Composite planar fabric of gouge from the Punchbowl Fault, California: *Journal of Structural Geology*, v. 9, p. 621–634, doi:10.1016/0191-8141(87)90147-7.
- Clark, M.M., and Lajoie, K.R., 1974, Holocene behavior of the Garlock fault: *Geological Society of America Abstracts with Programs*, v. 6, p. 156–157.
- Coles, S., Prothero, D.R., Quinn, J.P., and Swisher, C.C., III, 1997, Magnetic stratigraphy of the middle Miocene Boposta Formation, southern Sierra Nevada, California, in Girty, G.H., Hanson, R.E., and Cooper, J.D., eds., *Geology of the Western Cordillera: Perspectives From Undergraduate Research: Pacific Section SEPM (Society for Sedimentary Geology)*, v. 82, p. 21–34.
- Cox, B.F., 1982, Stratigraphy, sedimentology, and structure of the Goler Formation (Paleocene), El Paso Mountains, California: Implications for Paleogene tectonism on the Garlock fault zone [Ph.D. thesis]: Riverside, University of California, 248 p.
- Cox, B.F., and Diggles, M.F., 1986, Geologic map of the El Paso Mountains wilderness study area, Kern County, California: U.S. Geological Survey Miscellaneous Field Studies Map MF-1827, scale 1:24,000.
- Davis, G.A., and Burchfiel, B.C., 1973, Garlock fault: An intracontinental transform structure, southern California: *Geological Society of America Bulletin*, v. 84, p. 1407–1422, doi:10.1130/0016-7606(1973)84<1407:GFAITS>2.0.CO;2.
- Dibblee, T.W., Jr., 1952, Geology of the Saltdale quadrangle, California: California Division of Mines and Geology Bulletin 160, 66 p.
- Dibblee, T.W., Jr., 1967, Areal geology of the western Mojave Desert, California: U.S. Geological Survey Professional Paper 522, 153 p.
- Dokka, R.K., and Travis, C.J., 1990, Late Cenozoic strike-slip faulting in the Mojave Desert, California: *Tectonics*, v. 9, p. 311–340, doi:10.1029/TC009i002p0311.
- Fife, D.L., Ruff, R.W., and Unruh, M.E., 1988, Late Tertiary epithermal(?) gold mineralization associated with the Garlock fault zone, Christmas Canyon quadrangle, San Bernardino County, California, in Gregory, J., and Baldwin, E.J., eds., *Geology of the Death Valley Region: South Coast Geological Society Guidebook 16*, p. 397–407.
- Frankel, K.L., Glazner, A.F., Kirby, E., Monastero, F.C., Strane, M.D., Oskin, M.E., Unruh, J.R., Walker, J.D., Anandakrishnan, S., Bartley, J.M., Coleman, D.S., Dolan, J.F., Finkel, R.C., Greene, D., Kylander-Clark, A., Marrero, S., Owen, L.A., and Phillips, F., 2008, Active tectonics of the Eastern California shear zone, in Duebendorfer, E.M., and Smith, E.L., eds., *Field Guide to Plutons, Volcanoes, Reefs, Dinosaurs, and Possible Glaciation in Selected Areas of Arizona, California, and Nevada: Geological Society of America Field Guide 11*, p. 43–81, doi:10.1130/2008.fld011(03).
- Gan, W., Zhang, P., Shen, Z., Prescott, W.H., and Svarc, J.L., 2003, Initiation of deformation of the Eastern California Shear Zone: Constraints from the Garlock fault geometry and GPS observations: *Geophysical Research Letters*, v. 30, 1496, doi:10.1029/2003GL017090.
- Garfunkel, Z., 1974, Model for the late Cenozoic tectonic history of the Mojave Desert, California, and its relation to adjacent regions: *Geological Society of America Bulletin*, v. 85, p. 141–188, doi:10.1130/0016-7606(1974)85<1931:MFTLCT>2.0.CO;2.
- Glazner, A.F., Bartley, J.M., and Sanner, W.K., 2000, Nature of the southwestern boundary of the central Mojave Tertiary province, Rodman Mountains, California: *Geological Society of America Bulletin*, v. 112, p. 34–44, doi:10.1130/0016-7606(2000)112<34:NOTSBO>2.0.CO;2.
- Glazner, A.F., Walker, J.D., Bartley, J.M., and Fletcher, J.M., 2002, Cenozoic evolution of the Mojave block of southern California, in Glazner, A.F., Walker, J.D., and Bartley, J.M., eds., *Geologic Evolution of the Mojave Desert and Southwestern Basin and Range: Geological Society of America Memoir 195*, p. 19–41, doi:10.1130/0-8137-1195-9.19.
- Guest, B., Pavlis, T.L., Golding, H., and Serpa, L., 2003, Chasing the Garlock: A study of tectonic response to vertical axis rotation: *Geology*, v. 31, p. 553–556, doi:10.1130/0091-7613(2003)031<0553:CTGASO>2.0.CO;2.
- Harrison, T.M., and McDougall, I., 1981, Excess <sup>40</sup>Ar in metamorphic rocks from Broken Hill, New South Wales: Implications for <sup>40</sup>Ar/<sup>39</sup>Ar age spectra and the thermal history of the region: *Earth and Planetary Science Letters*, v. 55, p. 123–149, doi:10.1016/0012-821X(81)90092-3.
- Heizler, M.T., Perry, F.V., Crowe, B.M., Peters, L., and Appelt, R., 1999, The age of Lathrop Wells volcanic center: An <sup>40</sup>Ar/<sup>39</sup>Ar dating investigation: *Journal of Geophysical Research*, v. 104, p. 767–804, doi:10.1029/1998JB900002.
- Hess, F.L., 1910, Gold mining in the Randsburg quadrangle, California, in Hayes, C.W., and Lindgren, W., ed., *Contributions to Economic Geology: U.S. Geological Survey Bulletin 430-I*, p. 23–47.
- Hodges, K.V., McKenna, L.W., and Harding, M.B., 1990, Structural unroofing of the central Panamint Mountains, Death Valley region, southeastern California, in Wernicke, B.P., ed., *Basin and Range Extensional Tectonics near the Latitude of Las Vegas, Nevada: Geological Society of America Memoir 176*, p. 377–390, doi:10.1130/MEM176-p377.
- Hodges, K.V., Hames, W.E., Olszewski, W.J., Burchfiel, B.C., Royden, L.H., and Chen, Z., 1994, Thermobarometric and <sup>40</sup>Ar/<sup>39</sup>Ar geochronologic constraints on Eohimalayan metamorphism in the Dinggyé area, southern Tibet: *Contributions to Mineralogy and Petrology*, v. 117, p. 151–163, doi:10.1007/BF00286839.
- Holm, D.K., Geissman, J.W., and Wernicke, B.P., 1993, Tilt and rotation of the footwall of a major normal fault system: Paleomagnetism of the Black Mountains, Death Valley extended terrane, California: *Geological Society of America Bulletin*, v. 105, p. 1373–1387, doi:10.1130/0016-7606(1993)105<1373:TAROTF>2.3.CO;2.
- Hulin, C.D., 1925, Geology and ore deposits of the Randsburg quadrangle, California: California State Mining Bureau Bulletin 95, 152 p.
- Jahns, R.H., Troxel, B.W., and Wright, L.A., 1971, Some structural implications of a late Precambrian–Cambrian section in the Avawatz Mountains, California: *Geological Society of America Abstracts with Programs*, v. 3, p. 140.

- Lanphere, M.A., and Dalrymple, G.B., 1976, Identification of excess  $^{40}\text{Ar}$  by the  $^{40}\text{Ar}/^{39}\text{Ar}$  age spectrum technique: *Earth and Planetary Science Letters*, v. 32, p. 141–148, doi:10.1016/0012-821X(76)90052-2.
- Loomis, D.P., and Burbank, D.W., 1988, The stratigraphic evolution of the El Paso Basin, southern California: Implications for Miocene development of the Garlock fault and uplift of the Sierra Nevada: *Geological Society of America Bulletin*, v. 100, p. 12–28, doi:10.1130/0016-7606(1988)100<0012:TSEOTE>2.3.CO;2.
- Ludwig, K.R., 2012, Isoplot 3.75—A geochronological toolkit for Microsoft Excel: Berkeley Geochronology Center Special Publication 5, 74 p.
- Mancktelow, N.S., and Pavlis, T.L., 1994, Fold-fault relationships in low-angle detachment systems: *Tectonics*, v. 13, p. 668–685, doi:10.1029/93TC03489.
- Mattinson, J.M., 2005, Zircon U-Pb chemical abrasion (CA-TIMS) method: Combined annealing and multi-step partial dissolution analysis for improved precision and accuracy of zircon ages: *Chemical Geology*, v. 220, p. 47–66, doi:10.1016/j.chemgeo.2005.03.011.
- McGill, S., and Sieh, K., 1993, Holocene slip rate of the central Garlock fault in southeastern Searles Valley, California: *Journal of Geophysical Research*, v. 98, p. 14,217–14,231, doi:10.1029/93JB00442.
- McGill, S.F., Wells, S.G., Fortner, S.K., Kuzma, H.A., and McGill, J.D., 2009, Slip rate of the western Garlock fault, at Clark Wash, near Lone Tree Canyon, Mojave Desert, California: *Geological Society of America Bulletin*, v. 121, p. 536–554, doi:10.1130/B26123.1.
- Means, W.D., 1987, A newly recognized type of slickenside striation: *Journal of Structural Geology*, v. 9, p. 585–590, doi:10.1016/0191-8141(87)90143-X.
- Michael, E.D., 1966, Large lateral displacement on Garlock fault, California, as measured from offset fault system: *Geological Society of America Bulletin*, v. 77, p. 111–114, doi:10.1130/0016-7606(1966)77[111:LLDOGF]2.0.CO;2.
- Miller, D.M., and Yount, J.C., 2002, Late Cenozoic evolution of the north-central Mojave Desert inferred from fault history and physiographic evolution of the Fort Irwin area, California, in Glazner, A.F., Walker, J.D., and Bartley, J.M., eds., *Geologic Evolution of the Mojave Desert and Southwestern Basin and Range*: Geological Society of America Memoir 195, p. 173–197, doi:10.1130/0-8137-1195-9.173.
- Miller, M.M., Johnson, D.J., Dixon, T.H., and Dokka, R.K., 2001, Refined kinematics of the Eastern California shear zone from GPS observations, 1993–1998: *Journal of Geophysical Research*, v. 106, p. 2245–2263, doi:10.1029/2000JB900328.
- Monastero, F.C., Sabin, A.E., and Walker, J.D., 1997, Evidence for post-early Miocene initiation of movement on the Garlock fault from offset of the Cudahy Camp Formation, east-central California: *Geology*, v. 25, p. 247–250, doi:10.1130/0091-7613(1997)025<0247:EFPEMI>2.3.CO;2.
- Monastero, F.C., Walker, J.D., Katzenstein, A.M., and Sabin, A.E., 2002, Neogene evolution of the Indian Wells Valley, east-central California, in Glazner, A.F., Walker, J.D., and Bartley, J.M., eds., *Geologic Evolution of the Mojave Desert and Southwestern Basin and Range*: Geological Society of America Memoir 195, p. 199–228, doi:10.1130/0-8137-1195-9.199.
- Murdoch, J., and Webb, R.W., 1940, Notes on some minerals from southern California, II: *The American Mineralogist*, v. 25, p. 549–555.
- Noble, L.F., 1926, The San Andreas rift and some other active faults in the desert region of southeastern California: Carnegie Institute of Washington Year Book, v. 25, p. 415–428.
- Oskin, M., and Iriondo, A., 2004, Large-magnitude transient strain accumulation on the Blackwater fault, Eastern California shear zone: *Geology*, v. 32, p. 313–316, doi:10.1130/G20223.1.
- Peltzer, G., Crampe, F., Hensley, S., and Rosen, P., 2001, Transient strain accumulation and fault interaction in the Eastern California shear zone: *Geology*, v. 29, p. 975–978, doi:10.1130/0091-7613(2001)029<0975:TSAAFI>2.0.CO;2.
- Petit, J.P., 1987, Criteria for the sense of movement on fault surfaces in brittle rocks: *Journal of Structural Geology*, v. 9, p. 597–608, doi:10.1016/0191-8141(87)90145-3.
- Rittase, W.M., 2012, Neogene to Quaternary tectonics of the Garlock Fault and the Eastern California shear zone in the northern Mojave Desert, California [Ph.D. thesis]: Lawrence, University of Kansas, 224 p.
- Rittase, W.M., Kirby, E., McDonald, E., Walker, J.D., Gosse, J., Spencer, J.Q.G., and Herra, A.J., 2014, Temporal variations in Holocene slip rate along the central Garlock fault, Pilot Knob Valley, California: *Lithosphere*, v. 6, p. 48–58, doi:10.1130/L286.1.
- Sabin, A.E., 1994, Geology of the Eagle Crags volcanic field, northern Mojave Desert, China Lake Naval Air Weapons Station, California [Ph.D. thesis]: Golden, Colorado School of Mines, 209 p.
- Saleeby, J., Ducea, M.N., Busby, C., Nadin, E., and Wetmore, P.H., 2008, Chronology of pluton emplacement and regional deformation in the southern Sierra Nevada batholith, California, in Wright, J.E., and Shervais, J.W., eds., *Ophiolites, Arcs, and Batholiths: A Tribute to Cliff Hopson*: Geological Society of America Special Paper 438, p. 397–427, doi:10.1130/2008.2438(14).
- Samsel, H.S., 1962, Geology of the southeast quarter of the Cross Mountain quadrangle, Kern County, California: California Division of Mines and Geology Map Sheet 2, scale 1:39,350.
- Savage, J.C., Gan, W., and Svarc, J.L., 2001, Strain accumulation and rotation in the Eastern California Shear Zone: *Journal of Geophysical Research*, v. 106, p. 21,995–22,007, doi:10.1029/2000JB000127.
- Schermer, E., Luyendyk, B.P., and Cisowski, S., 1996, Late Cenozoic structure and tectonics of the northern Mojave Desert: *Tectonics*, v. 15, p. 905–932, doi:10.1029/96TC00131.
- Smith, E.I., Sanchez, A., Keenan, D.L., and Monastero, F.C., 2002, Stratigraphy and geochemistry of volcanic rocks in the Lava Mountains, California: Implications for the Miocene development of the Garlock fault, in Glazner, A.F., Walker, J.D., and Bartley, J.M., eds., *Geologic Evolution of the Mojave Desert and Southwestern Basin and Range*: Geological Society of America Memoir 195, p. 151–160, doi:10.1130/0-8137-1195-9.151.
- Smith, G.I., 1962, Large lateral displacement on the Garlock fault, California, as measured from an offset dike swarm: *The American Association of Petroleum Geologists Bulletin*, v. 46, p. 85–104.
- Smith, G.I., 1964, Geology and volcanic petrology of the Lava Mountains, San Bernardino County, California: U.S. Geologic Survey Professional Paper 457, 97 p.
- Smith, G.I., 1991, Anomalous folds associated with the east-central part of the Garlock fault, southeast California: *Geological Society of America Bulletin*, v. 103, p. 615–624, doi:10.1130/0016-7606(1991)103<0615:FAFATW>2.3.CO;2.
- Smith, G.I., and Kettner, K.B., 1970, Lateral displacement on the Garlock fault, southeastern California, suggested by offset sections of similar metasedimentary rocks, in Geological Survey Research 1970, Chapter D: U.S. Geological Survey Professional Paper 700-D, p. D1–D9.
- Smith, G.I., Troxel, B.W., Gray, C.H., Jr., and von Huene, R., 1968, Geologic reconnaissance of the Slate Range, San Bernardino and Inyo Counties, California: California Division of Mines and Geology Special Report 96, 33 p.
- Snyder, N.P., and Hodges, K.V., 2000, Depositional and tectonic evolution of a supradetachment basin:  $^{40}\text{Ar}/^{39}\text{Ar}$  geochronology of the Nova Formation, Panamint Range, California: *Basin Research*, v. 12, p. 19–30, doi:10.1046/j.1365-2117.2000.00108.x.
- Stewart, J.H., 1988, Tectonics of the Walker Lane belt, western Great Basin: Mesozoic and Cenozoic deformation in a shear zone, in Ernst, W.G., ed., *Metamorphism and Crustal Evolution of the Western United States*: Englewood Cliffs, New Jersey, Prentice-Hall, p. 681–713.
- Tchalenko, J.S., 1970, Similarities between shear zones of different magnitudes: *Geological Society of America Bulletin*, v. 81, p. 1625–1640, doi:10.1130/0016-7606(1970)81[1625:SBSZOD]2.0.CO;2.
- Topping, D.J., 1993, Paleogeographic reconstruction of the Death Valley extended region: Evidence from Miocene large rock-avalanche deposits in the Amargosa Chaos Basin, California: *Geological Society of America Bulletin*, v. 105, p. 1190–1213, doi:10.1130/0016-7606(1993)105<1190:PROTDV>2.3.CO;2.
- Unruh, J., and Hauksson, E., 2009, Seismotectonics of an evolving intracontinental plate boundary, southeastern California, in Oldow, J.S., and Cashman, P.H., eds., *Late Cenozoic Structure and Evolution of the Great Basin–Sierra Nevada Transition*: Geological Society of America Special Paper 447, p. 351–372, doi:10.1130/2009.2447(16).
- Walker, J.D., Black, R.A., Berry, A.K., Davis, P.J., Andrew, J.E., and Mitsdarfer, J.M., 2002, Geologic maps of the northern Mojave Desert and southwestern Basin and Range Province: Geological Society of America Memoir 195, p. 297–299, scale 1:250,000, doi:10.1130/0-8137-1195-9.297.
- Walker, J.D., Bidgoli, T.S., Didericksen, B.D., Stockli, D.F., and Andrew, J.E., 2014, Middle Miocene to recent exhumation of the Slate Range, eastern California, and implications for the timing of extension and the transition to transtension: *Geosphere*, v. 10, p. 276–291, doi:10.1130/GES00947.1.
- Whistler, D.P., Tedford, R.H., Takeuchi, G.T., Wang, W., Tseng, Z.L., and Perkins, M.E., 2009, Revised Miocene biostratigraphy and biochronology of the Dove Spring Formation, Mojave Desert, California: *Museum of Northern Arizona Bulletin*, v. 65, p. 331–362.
- Zhang, P., Ellis, M., Stemmmons, D.B., and Mao, F., 1990, Right-lateral displacements and the Holocene slip rate associated with prehistoric earthquakes along the southern Panamint Valley fault zone: Implications for southern Basin and Range tectonics and coastal California deformation: *Journal of Geophysical Research*, v. 95, p. 4857–4872, doi:10.1029/JB095iB04p04857.

SCIENCE EDITOR: CHRISTIAN KOEBERL  
ASSOCIATE EDITOR: STEFANO MAZZOLI

MANUSCRIPT RECEIVED 4 NOVEMBER 2013  
REVISED MANUSCRIPT RECEIVED 8 JUNE 2014  
MANUSCRIPT ACCEPTED 16 JULY 2014

Printed in the USA